Studies of aerosol particles performed with the MRI electron microscopes during the last three decades

Kikuo Okada[1], [*]

[1] Atmospheric Environment and Applied Meteorology Research Department, Meteorological Research Institute,
1-1 Nagamine, Tsukuba, Ibaraki 305-0052, Japan

*Corresponding author. Tel.: +81 29 853 8621; Fax: +81 29 855 7240, Email address: kokada@mri-jma.go.jp
(K. Okada)

During the last three decades, single-particle analyses have been carried out in the MRI by using a transmission electron microscope (Hitachi H-600 and H-6010) equipped with an energy-dispersive X-ray analyzer, and sometimes with a scanning electron microscope (Hitachi S-2150) as well. This report briefly describes the results obtained by these electron microscope studies.

1. Introduction

To evaluate the effect of aerosols on meteorological phenomena such as cloud formation and radiative transfer, it is important to study the composition and mixture state of individual aerosol particles. Many single-particle analyses have been carried out during the last three decades with the MRI electron microscope systems.

Here, the results obtained by using the MRI electron microscopes are briefly described.

2. Basic methods

Individual aerosol particles are usually collected on a carbon-coated nitrocellulose (collodion) film with aerosol samplers. Those collected on carbon film are usually coated with Pt/Pd alloy at a shadowing angle of 26.6° (arctan 0.5) and examined by a transmission electron microscope (TEM; Hitachi H-600 and H-6010) to assess their shape and volume.

The elemental composition of the collected particles is investigated by using the TEM equipped with an energy-dispersive X-ray (EDX) analyzer. The electron beams usually irradiate the central part of a particle with an accelerating voltage of 50 kV, and the X-ray spectrum is obtained through a Kevex UTW (ultra thin window) detector. Individual particles are quantitatively analyzed by the thin film method using Kevex Quantex[TM] software for energy-dispersive microanalysis.

3. Results and discussion
3.1. Modification of sea-salt particles

Sea-salt particles are one of the dominant types of particles originating from natural sources. In the atmosphere, sea-salt particles are modified by chemical reactions with acidic materials that result in emission of HCl from the particles.

The weight ratio of Cl to Na in seawater is mainly fixed at about 1.8. Therefore, examination of the Cl/Na weight ratio reveals whether the atmospheric sea-salt particles have been modified. Sea-salt particles with Cl/Na < 1 are regarded as having an apparent Cl deficiency (apparent modification). In the atmosphere over coastal regions, where sea-salt particles encounter anthropogenically polluted air, the composition of sea-salt particles is distinctively modified by chemical reactions with sulfuric acid and nitric acid [1-3].

The number percentages of sea-salt particles with Cl/Na < 1 in the radius range of 0.1–1 μm change spatially. For example, the number percentage at Shengshan Island, which is about 150 km east of Shanghai, was 18% [3], whereas the percentages at Marcus Island (24.3°N, 154.0°E) in the northwestern Pacific ranged from 6% to 36% [4]. The high percentage (36%) was associated with outflow from the Asian continent. In sea-salt particle samples collected by research ships during cruises [1, 5-8], the highest percentage (98%) was observed in the tropics near Borneo in association with biomass burning [1]. Thus, the number percentage of such particles changes depending on the trajectory of the air mass, and values were generally less than 10% in remote oceanic areas.

One study examined sea-salt particles collected at Syowa Station, Antarctica [9]. In the samples collected in austral summer, when the production of marine organosulfur is enhanced, the number fractions of sulfur-rich particles and modified sea-salt particles were high. In the samples collected in austral winter, when severe storms enhance the production of sea-salt particles, the number fraction of unmodified sea-salt particles was high. Another study investigated the concentration, number-size distribution, and

morphological features of aerosol particles (although not sea-salt particles) at Barrow, Alaska, in April 1997 [10]. That study found that new particle formation from the gas phase occurred in spite of the very low concentrations of gaseous materials, especially in air masses from the lower latitudes, and the accumulation mode included particles composed of sulfuric acid and ammonium sulfate.

A sample collected on 4 February 1991 near the sea surface in the South Pacific (10°S, 175°W) contained a very low percentage (4%) of sea-salt particles with Cl/Na < 1 [5]. Aircraft (Gulfstream 2) observations carried out nearby on 3 March 1990 at 11.2 km altitude by the International Strato/Tropospheric Air Chemistry (INSTAC-II) program [11] observed high aerosol concentrations in the upper part of cumulonimbus clouds with an optical particle counter (OPC). Both cloud-active and -inactive particles were transported vertically in the cumulonimbus clouds, and in these samples the number percentages of sea-salt particles in samples were large: 42% for particles with radii of 0.05–0.1 μm and 64% for particles with radii of 0.1–1 μm. This high abundance of sea salt in the smaller particles (radius < 0.1 μm) suggests that sea-salt particles play an important role in the cloudy marine atmosphere. EDX analysis showed that Cl/Na weight ratio in the sea-salt particles tended to decrease as excess sulfur increased. The number percentage of sea-salt particles with Cl/Na < 1 was 34% in the radius range of 0.1–1 μm, or about one order of magnitude higher than the percentage in the near-surface sample [5]. Thus, the sea-salt particles were modified during their vertical transport in cumulonimbus clouds. Other studies have also observed the vertical transport of sea-salt particles by convective clouds in the middle troposphere [12-14].

3.2. Elemental composition and shape of mineral particles (Asian dust) collected in three arid regions of China

In spring 1991, mineral particles (Asian dust) were collected with a battery-operated single-stage impactor in three arid regions of China (Hohhot, Inner Mongolia Autonomous Region; Zhangye, near the southern border of the Badain-Jaran Desert; and Qira, in the Taklamakan Desert) [15-17]. Compared with samples collected in Japan [18], the particles collected in these three locations usually showed that the edge of the particles were a distinct outline on the collection film.

Type classification of all particles with radii of 0.1–6 μm based on EDX analysis indicated that the number percentages of mineral particles were very high: 98.2% at Hohhot, 99.5% at Zhangye, and 99.1% at Qira). At Hohhot, fly ash particles (classified as mineral particles) accounted for 4.4% of aerosol particles.

The shape of 6998 mineral particles with radii between 0.1 and 6 μm at the three sites was examined by TEM [19]. In all three regions, the mineral particle shapes were irregular, with a median aspect ratio b/a (ratio of the longest dimension b to the orthogonal dimension a) of 1.4. Although

the aspect ratio exhibited no clear size dependence, the circularity factor ($4\pi S/l^2$; where S is surface area and l is periphery length) tended to decrease as the radius increased, suggesting that the larger sized particles included aggregated mineral particles. The particle height-to-width ratio h/a was also evaluated by measuring the length of a particle's shadow on the collection surface. The median h/a was 0.49 at Hohhot, 0.29 at Zhangye, and 0.23 at Qira. Analytical functions were fitted to the grand total of the frequency distributions of aspect ratios, height-to-width ratios, and circularity factors to allow parametric calculations of radiative effects and of the optical and sedimentation behavior of the mineral particles.

In another study, the influence of particle nonsphericity on the size distribution of submicrometer mineral particles as measured with an OPC was examined by comparison with TEM analysis obtained in a laboratory experiment and theoretical computations of light scattering by nonspherical particles [20]. When the size distribution of monodispersed mineral particles was compared between measurements made with the OPC and by TEM, the volume equivalent mode radii obtained with the OPC were 0.06–0.09 μm larger than those obtained by TEM.

The backscattering linear depolarization ratios of Asian and Saharan mineral dust, sea-salt, and ammonium sulfate particles were measured in a laboratory chamber to aid in the interpretation of polarization lidar measurements of tropospheric aerosols [21]. TEM results were also used in the study.

Electron micrographs of Asian dust particles in aerosols collected at Fukuoka, Japan, in March 2009 were used to produce a shape model for mineral dust particles for light scattering calculations [22]. In addition, local wind-blown mineral particles collected at Tsukuba were examined by TEM [23].

3.3. Modification of Asian dust-storm particles during long-range transport

Sea salt can modify mineral particles during long-range transport [24-26]. The abundance of dust-storm particles with radii > 1 μm internally mixed with sea salt were compared in samples from two dust-storm events observed in both Beijing, China, and Nagasaki, Japan, in spring 1991. In samples from the first event, 2% of Asian dust particles collected in Beijing on 30 April and 72% of those collected on 1 May in Nagasaki contained sea salt. In samples from the second event, 2% of dust particles collected on 7 and 9 May in Beijing and 16% of those collected in Nagasaki on 10 May included sea salt. The large abundance of Asian dust particles containing sea salt at Nagasaki during the first event was attributed to clouds encountered in the marine atmosphere during transport, which suggests that the mixed dust particles formed by cloud processes.

As previous research had suggested that sulfur accumulates on Asian dust particles [27], mineral particles from the

same dust episode were collected in April 1993 at both Beijing and Fukuoka [28]. Examination of individual dust particles by TEM showed that the dust particles collected in China had distinctly irregular shapes and contained low amounts of sulfur, whereas the dust particles collected over Japan after transport had been modified by the addition of sea salt and/or anthropogenic sulfur.

Asian dust particles were collected on a thin nitron ($C_{20}H_{16}N_4$) film in Nagoya, Japan, to detect nitrate ions [29]. TEM examination indicated that nitrate was present on the surface of dust particles collected during the dust-storm event. Nitrate and sulfate formation through heterogeneous reactions on the dust particles are one of the mechanisms of nitrogen oxides and sulfur dioxide removal from the atmosphere.

The presence of high fractions of mixed dust particles may enhance the cloud nucleating capability, as well as modulate its optical properties. As a result, the removal rate of Asian dust particles from the atmosphere might increase.

In addition to mineral particles, water-insoluble particles in rainwater at Shizuoka and Tsukuba, Japan, which were deposited directly onto electron microscope grids by ultracentrifugation [30], were found to consist of bacteria and leaf debris, and most of them were aggregated with mineral particles.

3.4. Mixing state of aerosol particles in the urban atmosphere

The composition and mixing properties of individual aerosol particles in the urban atmosphere must be known to evaluate the effect of anthropogenic aerosol particles on cloud formation and atmospheric radiation.

Aerosol particles were collected in 1989 in Katowice, Poland [31]. TEM results showed significant differences in the hygroscopic properties of aerosol particles that depended on the wind direction at the time of collection, which suggested that the aerosol particles were not well mixed and were influenced by the distribution of anthropogenic sources in Katowice and the surrounding area.

The mixing properties of individual aerosol particles with radii between 0.1 and 1 μm collected in 1991 in the urban atmosphere of Vienna, Austria [32], were studied by using water dialysis to extract water-soluble material. The averaged results showed that more than 85% of particles with radii between 0.1 and 0.7 μm were hygroscopic, and more than 50% of those with radii larger than 0.2 μm were mixed particles (hygroscopic particles with water-insoluble inclusions); mixed particles were dominant (80%) in the radius range of 0.5–0.7 μm. Moreover, the number proportion of mixed particles increased with increasing radius, and their abundance also increased as the particle mass loading in the atmosphere increased. The volume fraction of water-soluble material (ε) in mixed particles tended to decrease with increasing radius, implying that the mixed particles formed by heterogeneous processes such as condensation and surface reactions.

The mixing properties of individual aerosol particles with radii of 0.02–0.2 μm collected with an electrostatic aerosol sampler in June 2000 at Tsukuba [33] were studied by using water dialysis. The proportions of particles with water-soluble material (hygroscopic particles) ranged from 20% to 80% in the whole radius range and tended to increase with increasing radius. Moreover, morphological examination revealed two types of soot-containing particles: externally mixed (pure) and internally mixed soot particles. The number fractions of internally mixed soot particles increased with increasing radius. A sample collected in "polluted" air showed that internally mixed soot particles were dominant (number fraction, 75%) in the larger radius range of 0.1–0.2 μm.

At Tsukuba, aerosol particles in ambient air downstream of a differential mobility analyzer (DMA) were measured with an impactor at the electrical mobility radii of 0.1, 0.15, and 0.2 μm in dry conditions (relative humidity < 3%) [34-36]. The particles were collected on a film covered with silicone oil and examined by TEM to determine their diameters, shapes, and morphological changes caused by electron-beam bombardment. Measurements with an OPC were carried out in parallel to assess the abundance of externally mixed soot particles. Most of the number frequency distributions obtained by TEM peaked at the DMA diameters (mobility diameters). Circularity factors of pure soot particles decreased as the particle radius increased, and their irregular shapes produced broad size-frequency distributions. Comparison of soot particle abundance between the OPC and TEM results showed good agreement.

With regard to cloud formation, the efficiency of nucleation scavenging of aerosol particles with radii between 0.028 and 0.28 μm was measured at Tsukuba by using two thermal gradient diffusion chambers, one with and one without a water vapor source [37]. The efficiencies were measured as a function of the supersaturation of water vapor (*S*). The mean efficiency by aerosol volume was high (0.75–0.93) at *S* of 0.25–1.04%. The efficiencies were closely related to the hygroscopic properties of the aerosol particles as determined by electron microscopy. Electron microscope studies of aerosol particles in clouds and fog were also performed [38-42].

The light absorption property of carbonaceous particles was investigated at Tsukuba in relation to the mixing state [43]. The volume fraction of water-soluble material (ε) in soot-containing particles was evaluated by comparing electron micrographs before and after water dialysis. The mass absorption coefficient (unit; $m^2\ g^{-1}$) tended to increase with the average ε in soot-containing particles with radii of 0.05–0.5 μm. Thus, coatings of water-soluble material around soot particles enhance the absorption of solar radiation.

Internal mixtures of nitrate with sulfate in urban aerosol particles were examined by using the vapor-deposited thin nitron film method and EDX analysis [44].

3.5. Free tropospheric aerosol particles

Aircraft observations are used to study aerosols in the free troposphere. The INSTAC program, mentioned in section 3.1, is one example. Another is a series of the Pacific Atmospheric Chemistry Experiment (PACE) campaigns, jointly carried out by the MRI and the Australian Commonwealth Scientific and Industrial Research Organisation (CSIRO).

In the PACE I campaign, individual aerosol particles were collected at 5–6 km altitude in the middle troposphere over the western Pacific Ocean between Melbourne (38°S) and Sendai (38°N) in January 1994 [14]. By EDX analysis and morphological identification, particles were classified into various types, including sea salt, mineral, sulfate, and sulfuric acid. Sulfuric acid and ammonium sulfate, which were commonly found in particles of 0.1–1 μm radius across most of the observed region, were considered important background aerosols. Sea-salt particles were also often abundant in the tropical regions (present at up to 67%), owing to vertical transport by convective clouds. North of 20°N, mineral particles were dominant, suggesting transport of Asian dust particles in the westerly air stream. Abundant Asian dust particles covered with sulfuric acid indicated that modification of Asian dust particles had occurred.

A local flight over Saipan, a subtropical area, carried out during the PACE I campaign [45] showed that the number concentration of condensation nuclei (CN) increased with altitude in contrast to large particle concentrations, which decreased with altitude. Most particles collected at 6 km altitude were composed of sulfuric acid, suggesting that new particle formation is favored in the upper troposphere.

In the PACE III campaign, individual aerosol particles were collected at 5–6 km altitude in the middle troposphere between Melbourne and Sendai, as in the PACE I campaign, but in July 1995 [46]. The PACE III campaign results were similar to the PACE I results, except that mineral particles were absent in the northern mid-latitudes and spatial shifts in particle composition and concentrations were observed. Comparison of the results of the two campaigns suggested that seasonal shifts in the locations of the intertropical convergence zone and wind belts contributed to the seasonal differences in the spatial distributions of particles in the middle troposphere over the western Pacific.

During the PACE V campaign over Kalimantan, Indonesia, in October 1997, individual particles were collected from a very dense haze caused by Indonesian forest fires [47, 48]. Although 60–90% of the particles collected at altitudes of 1–5 km contained K, the S/K weight ratio was high, with median values of 9–18, independent of particle size. These ratios were much larger than those (median values of 2–4) measured in haze from biomass burning in

northern Australia. The high weight ratios over Kalimantan were attributed to the heterogeneous growth of particles through the oxidation of SO_2. In addition to SO_2 from the combustion of forest biomass, SO_2 originating from the combustion of buried peat was believed to have also contributed to the high S/K ratios. The samples were also examined by electron microscopy after using water dialysis to extract water-soluble material, and benzene dialysis to extract organic material. Individual aerosol particles with radii of 0.1–2 μm were mainly present as an internal mixture of water-soluble organic material and inorganic salt (mainly ammonium sulfate). Chain aggregations of electron-opaque spherules (elemental carbon) were also found, but their proportion was small.

In the PACE VII campaign in February 2000 [49], the number-size distributions of aerosols with radii between 0.05 and 5 μm were observed in the free troposphere up to 11 km altitude in different air masses over the western and northwestern Pacific Ocean. The results showed that over the northern mid-latitudes, Asian outflow contained many anthropogenic particles.

During the PACE II campaign (October 1994), soot particles originating from biomass burning were collected in the middle troposphere over Australia [50]. The abundance of internally mixed soot particles tended to increase with particle radius, and internally mixed soot particles composed 88% of particles with radii of 0.1–0.35 μm.

Soot particles emitted from several hundred oil-well fires in Kuwait from February 1991 were collected by aircraft on 27 April 1991 at 7.5 km altitude over Tsukuba [51, 52]. The number percentage of soot-containing particles was high (53%) in the radius range of 0.15–1 μm. Moreover, about 90% of the soot particles were covered with water-soluble material. From the backward- and forward-trajectory analyses of air parcels, the soot particles over Japan would be supplied to the upper troposphere in the first half of April and those have circled the globe before arrival at sampling point.

Aerosol particles collected by aircraft in January 1983 in the upper troposphere (7.2 km altitude) over Showa Station, Antarctica, were examined by EDX analysis [53]. The number percentage of mineral particles was high (74%) for particles with radii between 0.1 and 1.6 μm. The transport pathways of the mineral particles were studied by 3-D trajectory analyses of U. S. National Meteorological Center (NMC) data, which are reported twice daily. Most aerosol particles collected in the Antarctic upper troposphere originated from El Chichon volcano and had been transported downward from the stratosphere over Antarctica.

Aerosol particles for examination by electron microscopy have also been collected at a mountain site [54, 55], and from the upper troposphere and stratosphere by balloon-borne samplers [56-59].

1   Mouri, H., I. Nagao, K. Okada, S. Koga and H. Tanaka, 1996: Elemental composition of individual aerosol particles collected from the coastal marine boundary layer. *J. Meteor. Soc. Japan*., **74**, 585-591.

2   Roth, B. and K. Okada, 1998: On the modification of sea-salt particles in the coastal atmosphere. *Atmos. Environ*, **32**, 1,555-1,569.

3   Li, F., and K. Okada, 1999: Diffusion and modification of marine aerosol particles over the coastal areas in China - a case study using a single particle analysis. *J. Atmos. Sci*., **56**, 241-248.

4   Naoe, H.. and K. Okada, 2006. Modification of sea-salt particles in the remote marine atmosphere in the North Pacific. *Pap. Meteor. Geophys*, **57**, 47-54.

5   Mouri, H.., K. Okada and K. Shigehara, 1993: Variation of Mg, S, K and Ca contents in individual sea-salt particles. *Tellus*, **45B**, 80-85.

6   Mouri, H. and K. Okada, 1993: Shattering and modification of sea-salt particles in the marine atmosphere. *Geophys. Res. Lett*., **20**, 49-52.

7   Mouri, H., K. Okada and S. Takahashi, 1995: Giant sulfur-dominant particles in remote marine boundary layer. *Geophys. Res. Lett*., **22**, 595-598.

8   Mouri, H., I. Nagao, K. Okada, S. Koga and H. Tanaka, 1997: Elemental composition of individual aerosol particles collected over the Southern Ocean: A case study. *Atmos. Res*., **43**, 183-195.

9   Mouri, H., I. Nagao, K. Okada, S. Koga and H. Tanaka, 1999: Individual-particle analyses of coastal Antarctic aerosols. *Tellus*, **51B**, 603-611.

10 Zaizen, Y., K. Okada, M. Ikegami, T. Aoki, Y. Sawa, F. Nishio and Y. Tachibana, 1998: Size distribution of aerosols at Barrow in Alaska - A case study in spring. *Polar Meteor. Glaciol*., **12**, 40-48.

11 Ikegami, M., K. Okada, Y. Zaizen and Y. Makino, 1994: Sea-salt particles in the upper tropical troposphere. *Tellus*, **46B**, 142-151.

12 Ikegami, M., K. Okada, Y. Zaizen and Y. Makino, 1993: Aerosol particles in the middle troposphere over the northwestern Pacific. *J. Meteor. Soc. Japan*, **71**, 517-528.

13 Ikegami, M., K. Okada and Y. Zaizen, 1991: Sea-salt particles in the middle troposphere over the tropical Pacific Ocean. *Pap. Meteor. Geophys*, **42**, 31-41.

14 Ikegami, M., K. Okada, Y. Zaizen, Y. Tsutsumi, Y. Makino, J. B. Jensen and J. L. Gras, 2004: The composition of aerosol particles in the middle troposphere over the western Pacific Ocean: Aircraft observations from Australia to Japan, January 1994. *Atmos. Environ*, **38**, 5,945-5,956. (Erratum: *Atmos. Environ*., **40**, 793, 2006)

15 Okada, K., Y. Qin and K. Kai, 2005: Elemental composition and mixing properties of atmospheric mineral particles collected in Hohhot, China. *Atmos. Res*., **73**, 45-67.

16 Okada, K. and K. Kai, 1995: Features and elemental composition of mineral particles collected in Zhangye, China. *J. Meteor. Soc. Japan*, **73**, 947-957.

17 Okada, K. and K. Kai, 2004: Atmospheric mineral particles collected at Qira in the Taklamakan Desert, China. *Atmos. Environ*, **38**, 6,927-6,935.

18 Okada, K., A. Kobayashi, Y. Iwasaka, H. Naruse, T. Tanaka and O. Nemoto, 1987: Features of individual Asian dust-storm particles collected at Nagoya, Japan. *J. Meteor. Soc. Japan*, **65**, 515-521.

19 Okada, K., J. Heintzenberg, K. Kai and Yu Qin, 2001: Shape of atmospheric mineral particles collected in three Chinese arid-regions. *Geophys. Res. Lett.,* **28**, 3,123- 3,126**.**

20 Sakai, T., Y. Zaizen, C. Nishita, A. Matsuki, Y. Mano and K. Okada, 2008: Influence of particle nonsphericity on the size distribution measurement of submicrometer mineral dust by use of optical particle counter. Earozoru Kenkyu (formerly: *J. Aerosol Research Japan*), **23**, 269-277.

21 Sakai, T., T. Nagai, Y. Zaizen and Y. Mano, 2010: Backscattering linear depolarization ratio measurements of mineral, sea-salt, and ammonium sulfate particles simulated in a laboratory chamber. *Applied Optics*, **49**, 4,441-4,449.

22 Ishimoto, H., Y. Zaizen, A. Uchiyama, K. Masuda and Y. Mano, 2010: Shape modeling of mineral dust particles for light-scattering calculations using the spatial Poisson-Voronoi tessellation. *J. Quan. Spec. Rad. Trans*, **111**, 2434-2443.

23 Okada, K. and M. Ikegami, 2002: A case study of local wind-blown dust observed in Tsukuba, Japan. *Pap. Meteor. Geophys*, **52**, 9-18.

24 Niimura, N., K. Okada, X.-B. Fan, K. Kai, K. Arao and G.-Y. Shi, 1994: A method for the identification of Asian dust-storm particles mixed internally with sea salt. *J. Meteor. Soc. Japan*, **72**, 777-784.

25 Fan, X.-B., K. Okada, N. Niimura, K. Kai, K. Arao, G.-Y. Shi, Y. Qin and Y. Mitsuta, 1996: Mineral particles collected in China and Japan during the same Asian dust-storm event. *Atmos. Environ*, **30**, 347-351.

26 Niimura, N., K. Okada, X.-B. Fan, K. Kai, K. Arao, G.-Y. Shi and S. Takahashi, 1998: Formation of Asian dust-storm particles mixed internally with sea salt in the atmosphere. *J. Meteor. Soc. Japan*, **76**, 275-288.

27 Okada, K., H. Naruse, T. Tanaka, O. Nemoto, Y. Iwasaka, P.-M. Wu, A. Ono, R. A. Duce, M. Uematsu, J. T. Merrill and K. Arao, 1990: X-ray spectrometry of individual Asian dust-storm particles over the Japanese islands and the North Pacific Ocean. *Atmos. Environ*, **24A**, 1369-1378.

28 Zhou, M., K. Okada, F. Qian, P.-M. Wu, L. Su, B. E. Casareto and T. Shimohara, 1996: Charactersitics of dust storm particles and their long-range transport from China to Japan - Case studies in April 1993. *Atmos. Res*., **40**, 19-31.

29 Wu, P.-M. and K. Okada, 1994: Nature of coarse nitrate particles in the atmosphere- -A single particle approach. *Atmos. Environ*, **28**, 2053-2060.

30 Casareto, B. E., Y. Suzuki, K. Okada and M. Morita, 1996: Biological micro- particles in rain water. *Geophys. Res. Lett*., **23**, 173-176.

31 Pastuszka, J. S. and K. Okada, 1995: Features of atmospheric aerosol particles in Katowice, Poland. *Sci. Total Environ*, **175**, 179-188.

32 Okada, K. and R. M. Hitzenberger, 2001: Mixing properties of individual submicrometer aerosol particles in Vienna. *Atmos. Environ*, **35**, 5617-5628.

33 Naoe, H. and K. Okada, 2001: Mixing properties of submicrometer aerosol particles in the urban atmosphere - with regard to soot particles. *Atmos. Environ*, **35**, 5765-5772.

34 Heintzenberg, J., K. Okada and B. P. Luo, 2002: Distribution of optical properties among atmospheric submicrometer particles of given electrical mobilities. *J. Geophys. Res*., **107**, doi: 10.1029/2001JD000372

35 Okada, K. and J. Heintzenberg, 2003: Size distribution, state of mixture and morphology of urban aerosol particles at given electrical mobilities. *J. Aerosol Sci*., **34**, 1,539-1,553.

36 Heintzenberg, J., K. Okada, T. Trautmann and P. Hoffmann, 2004: Modeling of the signals of an optical particle counter for real nonspherical particles. *Applied Optics*, **43**, 5,893-5,900.

37 Okada, K., T. Tanaka, H. Naruse and T. Yoshikawa, 1990: Nucleation scavenging of submicrometer aerosol particles. *Tellus*, **42B**, 463-480.

38 Naruse, H. and K. Okada, 1989: Change in concentrations of cloud condensation nuclei and aerosol particles during the dissipation of fog. *Pap. Meteor. Geophys*, **40**, 125-137.

39 Akagawa, H. and K. Okada, 1993: Sizes of cloud droplets and cloud droplet residues near stratus cloud base. *Atmos. Res*., **30**, 37-49.

40 Hallberg, A., J. A. Ogren, K. J. Noone, K. Okada, J. Heintzenberg and I. B. Svenningsson, 1994: The influence of aerosol particle composition on cloud droplet formation. *J. Atmos. Chem*., **19**, 153-171.

41 Heintzenberg, J., K. Okada and J. Ström, 1996: On the composition of non-volatile material in upper tropospheric aerosols and cirrus crystals. *Atmos. Res*., **41**, 81- 88.

42 Ueda, S., K. Osada and K. Okada, 2011: Mixing states of cloud interstitial particles between water-soluble and insoluble materials at Mt. Tateyama, Japan: Effects of meteorological conditions. *Atmos. Res*., **99**, 325-336.

43 Naoe, H., S. Hasegawa, J. Heintzenberg, K. Okada, A. Uchiyama, Y. Zaizen, E. Kobayashi and A. Yamazaki, 2009: State of mixture of atmospheric submicrometer black carbon particles and its effect on particulate light absorption. *Atmos. Environ*, **43**, 1,296-1,301.

44 Wu, P.-M., A. Ono and K. Okada, 1987: On the mixture of submicrometer nitrate- containing particles in the urban atmosphere. *J. Meteor. Soc. Japan*, **65**, 1005- 1010.

45 Zaizen, Y., M. Ikegami, Y. Tsutsumi, Y. Makino, K. Okada, J. Jensen and J. L. Gras, 1996: Number concentration and size distribution of aerosol particles in the middle troposphere over the western Pacific Ocean. *Atmos. Environ*, **30**, 1755- 1762.

46 Okada, K., M. Ikegami, Y. Zaizen, Y. Tsutsumi, Y. Makino, J. B. Jensen and J. L. Gras, 2008: Submicrometer sulfur-rich particles in the middle troposphere: Aircraft observations from Australia to Japan. *Atmos. Res.*, **88**, 185-198.

47 Ikegami, M., K. Okada, Y. Zaizen, Y. Makino, J. B. Jensen, J. L. Gras and H. Harjanto, 2001: Very high weight ratios of S/K in individual haze particles over Kalimantan during the 1997 Indonesian forest fires. *Atmos. Environ*, **35**, 4237- 4243.

48 Okada, K., M. Ikegami, Y. Zaizen, Y. Makino, J. B. Jensen and J. L. Gras, 2001: The mixture state of individual aerosol particles in the 1997 Indonesian haze episode. *J. Aerosol Sci.*, **32**, 1269-1279. (Erratum: *J. Aerosol Sci.*, **33**, 553, 2002)

49 Zaizen, Y., K. Okada, M. Ikegami, Y. Sawa and Y. Makino, 2004: Number-size distributions of aerosol particles in the free troposphere over the northwestern Pacific Ocean - Influence of Asian outflow and tropical air transport. *J. Meteor. Soc. Japan*, **82**, 1147-1160.

50 Okada, K., M. Ikegami, Y. Zaizen, Y. Tsutsumi, Y. Makino, J. B. Jensen and J. L. Gras, 2005: Soot particles in the free troposphere over Australia. *Atmos. Environ*, **39**, 5079-5089.

51 Okada, K., M. Ikegami, O. Uchino, Y. Nikaidou, Y. Zaizen, Y. Tsutsumi and Y. Makino, 1992: Kuwaiti soot over Japan. *Nature*, **355**, 120.

52 Okada, K., M. Ikegami, O. Uchino, Y. Nikaidou, Y. Zaizen, Y. Tsutsumi and Y. Makino, 1992: Extremely high proportions of soot particles in the upper troposphere over Japan. *Geophys Res. Lett*, **19**, 921-924.

53 Yamazaki, K., K. Okada and Y. Iwasaka, 1989: Where do aerosol particles in the Antarctic upper troposphere come from? - A case study in January 1983. *J. Meteor. Soc. Japan*, **67**, 889-906.

54 Naoe, H., J. Heintzenberg, K. Okada, Y. Zaizen, K. Hayashi, T. Tateishi, Y. Igarashi, Y. Dokiya and K. Kinoshita, 2003: Composition and size distribution of submicrometer aerosol particles observed on Mt Fuji in the volcanic plumes from Miyakejima. *Atmos. Environ*, **37**, 3047-3055.

55 Naoe, H., Y. Zaizen. K. Yanagida, K. Okada, H. Takahashi and Y. Igarashi, 2012: Mixing state of aerosol particles at Mt. Hotaka, Japan: A case study in winter. *Atmos. Res.*, **118**, 170-179.

56 Mouri, H., K. Okada and Y. Tazawa, 1992: Stratospheric solid particles collected at 24 km altitude over Japan using a balloon-borne impactor. *J. Meteor. Soc. Japan*, **70**, 67-75.

57 Wu, P.-M., K. Okada, T. Tanaka, T. Sasaki, T. Nagai, T. Fujimoto and O. Uchino, 1994: Balloon observation of stratospheric aerosols over Tsukuba, Japan: Two years after the Pinatubo volcanic eruption. *J. Meteor. Soc. Japan*, **72**, 475-480.

58 Okada, K., P.-M. Wu, T. Tanaka and M. Hotta, 1997: A light balloon-borne sampler collecting stratospheric aerosol particles for electron microscopy. *J. Meteor. Soc. Japan*, **75**, 753-760.

59 Xu, L., K. Okada, Y. Iwasaka, K. Hara, K. Okuhara, Y. Tsutsumi and G.-Y. Shi, 2001: On the composition of individual aerosol particle in the troposphere and stratosphere over Xianghe (39.45°N, 117.0°E), China. *Atmos. Environ*, **35**, 3,145-3,153.

Modification of dust particles by sea salt adherence and surface chemical reactions in the marine atmosphere

Daizhou Zhang[1,*], Guangyu Shi[2] and Yasunobu Iwasaka[3]

[1]Prefectural University of Kumamoto, Kumamoto 862-8502, Japan
[2]Institute of Atmospheric Physics, Chinese Academy of Science, Beijing 100029, China
[3]FSO, Kanazawa University, Kanazawa 920-1192, Japan

*Corresponding author. Tel.: +81 96 387 6712; Fax: +81 96 384 6765, Email address: dzzhang@pu-kumamoto.ac.jp (D. Zhang)

Modifications to dust particles in the marine atmosphere detected by electron microscopy are briefly reviewed. Two processes are emphasized: the interaction of particles with gaseous species leading to the formation of chloride, sulfate, and nitrate, and the adherence of sea salt to particles.

Keywords: Mineral dust; Marine atmosphere; Long-range transport; Environmental subsequent effects

1. Introduction

Individual aerosol particle analysis can provide accurate information on the shape, size, composition, and other properties of particles. Unlike bulk, or integrated, sample analysis, which shows quantitative characteristics of all particles collected on a filter, individual particle analysis reveals the physical and chemical nature of a single atmospheric particle. Because it is tremendously time consuming and expensive, however, and because suitable standards are lacking, it is very hard to obtain good-quality quantitative data, although this situation is gradually improving owing to the commercial use of aerosol time-of-flight mass spectrometry (ATOFMS) in a limited series of field studies.

Here, dust particle changes that occur during transport in the atmosphere, caused by the formation of sulfate, nitrate, and chloride and by adherence of sea salt, are summarized, and their effects on the properties and fate of the dust particles are examined. In addition, important gaps in our knowledge and current topics of study relevant to individual particle analysis, as well as the potential subsequent environmental effects, are briefly described.

2. Sulfate, nitrate, and chloride formation

The formation of particulate sulfate and nitrate is substantially enhanced by the presence of dust particles in the atmosphere. Observations of Asian dust made at different sites, from dust source areas to remote marine areas, have shown that as the distance traveled by a dust plume increases, the number of sulfate- and nitrate-containing particles also increases. Furthermore, the formation of such compounds is much more efficient in the marine atmosphere than in the continental atmosphere, an effect that can be attributed to the greater humidity in the marine atmos-

phere. Although mineral dust containing substantial sulfate and/or nitrate has been reported in the urban atmosphere of Chinese cities, the weather conditions and records obtained at the time of sample collection indicate that these mineral particles were probably not from desert areas; more likely they derived from areas with active anthropogenic emissions such as road dust and coal burning emissions.

Moreover, the uptake of sulfate and nitrate by dust particles depends on the particle mineralogy; nitrate accumulation is more likely on calcium-rich particles, and sulfates tend to accumulate on aluminosilicate-rich dust. Further, the formation of nitrate on mineral particles relates mainly to their calcium carbonate content rather than to their silicon dioxide content.

The formation of sulfate on dust particles does not increase their hygroscopicity, whereas nitrate formation can remarkably increase particle hygroscopicity. The presence of nitrate on dust particles can also change the particles from hydrophobic to hydrophilic when the relative humidity is less than 30%, as shown by both laboratory studies and field measurements. Thus, the formation of nitrate on dust particles might increase their potential to act as cloud condensation nuclei (CCN) to produce cloud droplets.

A series of observations, for example, by ATOFMS, has provided evidence of hydrogen chloride (HCl) formation and deposition on dust particles in the marine atmosphere. HCl is a secondary acid released from sea salt by substitution reactions.

Ongoing analyses have shown that, in the absence of substantial sulfate and nitrate (i.e., in air masses less polluted by anthropogenic emissions), the effects of chloride formation on dust particles are likely important. Chloride on dust particles can also remarkably increase their hygrosco-

picity, suggesting that the chlorine-related chemistry of dust particles might substantially increase the ability of dust particles to act as CCN at high altitudes in the marine atmosphere. In addition, a recent report indicated that dust particles coated with organic acidic materials could more efficiently act as CCN.

3. Dust particles with adhering sea salt

Mineral dust particles frequently become mixed with sea salt during their transport in the marine boundary layer, and the mixed particles differ from mineral dust in size, hygroscopicity, and other physical-chemical characteristics.

Observational data and theoretical calculations have shown that the adherence of sea salt to dust particles can substantially enhance the settling of the particles. As a result, mixed particles composed of dust and sea salt are removed from the atmosphere faster than dust particles without sea salt. Since sea salt derives from sea spray, mixed particles are mainly found in the marine atmosphere. Thus, the gravitational settling of dust particles to the sea surface is fundamentally different from the settling of particles to the ground surface from the continental atmosphere. This sea salt effect on dust settling must therefore be taken into account to correctly map dust fluxes to the ocean. Studies comparing the effects of sulfate and sea salt on dust particles have shown that sulfate and nitrate formation on dust particles influences particle settling less than sea salt.

Unfortunately, the mechanism responsible for the mixing of dust and sea salt has yet to be elucidated. Coagulation of dust particles and sea salt particles that collide as a result of Brownian motion cannot explain the observed frequency of mixed particles, suggesting that some unknown process causes dust and sea salt mixing. Mixing in clouds has been suggested, but it cannot explain observations obtained during high-pressure conditions. Small-scale turbulences in the convective unstable mixed layer probably play a very important role in determining the fate of dust particles in the marine boundary layer. Horizontal roll vortices and streaks may alter the settling process to one very different from gravitational settling and delay the removal of particles, consequently increasing the likelihood that they will mix with gaseous species and other particulate matter.

Mixed particles of mineral dust and sea salt show stronger hydrophobicity than mineral dust particles. However, this characteristic is attributed to the sea salt component of the particles, which shows very strong hygroscopicity

In addition, when sea salt becomes mixed with mineral dust it may be less likely to lose chloride ions, as a result of the deposition of acidic materials such as sulfate and nitrate on the dust. This effect is plausible because most mineral dust particles are alkaline.

4. Remaining questions and challenges

Settling dust particles have an important influence on marine ecosystems by supplying nutrients such as iron. Early integrated sample analyses have shown that the iron in dust particles is water soluble. How much and by what processes the iron in dust particles becomes bioavailable is as yet unknown. Laboratory experiments have shown that the formation of acidic sulfate and nitrate materials can transform iron from a water-insoluble to a water-soluble form, although the experimental conditions differed greatly from those in the atmosphere. Model simulations have also evaluated these integrated sample results, but evidence from single particle analysis is not yet available.

Recent studies of integrated samples have reported that during long-distance transport in the atmosphere dust particles may become mixed with compounds such as halocarbons and polycyclic aromatic hydrocarbons and these mixed particles may importantly affect Earth geochemical cycles. However, methods have not yet been developed to detect these compounds on individual particles.

Atmospheric dust dispersion may play a role in the evolution and conservation of microorganism diversity in the natural environment. Some recent studies using culturing and staining techniques coupled with bioassays have confirmed that the abundance of microorganisms increases when there are dust plumes in the ambient air. However, methods to identify the microorganisms on a single particle are not available; consequently, whether microorganisms occur on dust particles is not clear, although it seems plausible, or even, probable, that they should.

Aerosol particle shape revealed by transmission electron microscopy and the implications for its optical properties

Kouji Adachi[1]

[1]Meteorological Research Institute, 1-1 Nagamine, Tsukuba, Ibaraki 305-0052, Japan

Corresponding author. Tel.: +81 29 853 8570, Email address: adachik@mri-jma.go.jp (K. Adachi)

Aerosol particles in the atmosphere have various shapes, and their shape greatly influences light scattering and absorption by the particles. Direct observation by electron microscopy, including transmission electron microscopy (TEM), can reveal particle shapes. Current TEM techniques can determine the two-dimensional and three-dimensional shapes and hygroscopicity of aerosol particles. Optical properties of non-spherical three-dimensional aerosol particles with multiple components can be determined by using discrete dipole approximation (DDA). Here, I show how the combination of TEM techniques and DDA calculations can be used to determine the shape and configuration, and thus the optical properties, of realistic aerosol particles.

1. Introduction

Atmospheric aerosol particles viewed by transmission electron microscopy (TEM) show various shapes, including fractal, aggregate, cubic, plate-like, and spherical. However, Mie theory, which is commonly used to estimate the optical properties of particles (e.g., absorption, scattering, and the asymmetry parameter), assumes that the particles are spherical. Here, I show the use of a discrete dipole approximation (DDA) calculation to determine the optical properties of non-spherical particles and electron tomography to determine the three-dimensional (3D) shapes and configurations of aerosol particles. I show several examples of the optical properties of non-spherical aerosol particles.

2. Material and methods

The electron tomography and DDA methods are described in detail by Adachi et al. (2010: Ref. 1) .

3. Results and discussion
3.1. Soot particle shape and configuration

Soot particles commonly have a fractal shape and are mixed with other particles. The amount of light absorption by a soot particle depends on its 3D shape and configuration. Adachi et al. (2010: Ref. 1) showed the effects of coatings on soot particles and particle configuration by simulating different particle shapes and coatings. Here, I describe how soot particle shape and configuration affect light absorption.

Coating enhances light absorption by soot particles [2]

via a lens effect (Figure 1). Because of refraction of light within the coating, more light is focused on a coated soot particle than on one without coating.
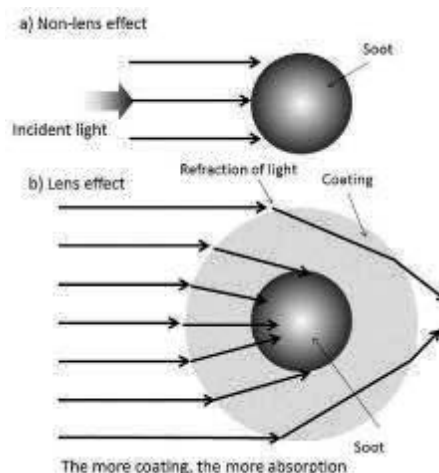
Figure 1 Schematic model of the lens effect. Light absorption by a) non-coated and b) coated soot particle.

The position of the soot within the coating determines the amount of light absorption [3]. Light tends to be focused on the center of the entire particles in the size range of ambient aerosol particles. Thus, when soot particles are centered within the coating, they absorb more light than when they are closer to one edge (Figure 2).
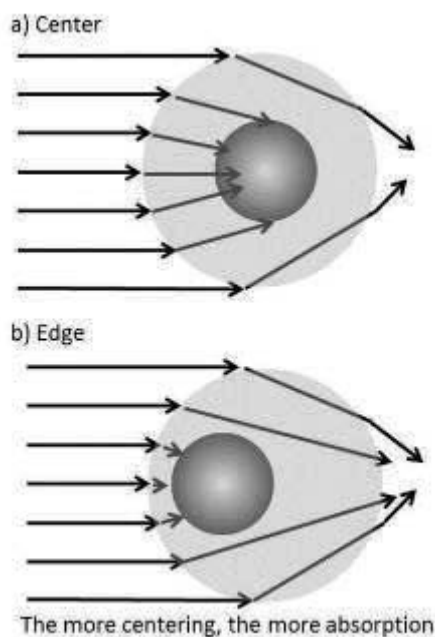
Figure 2 Schematic diagram of the position effect. Soot a) centered within and b) near the edge of the coating.
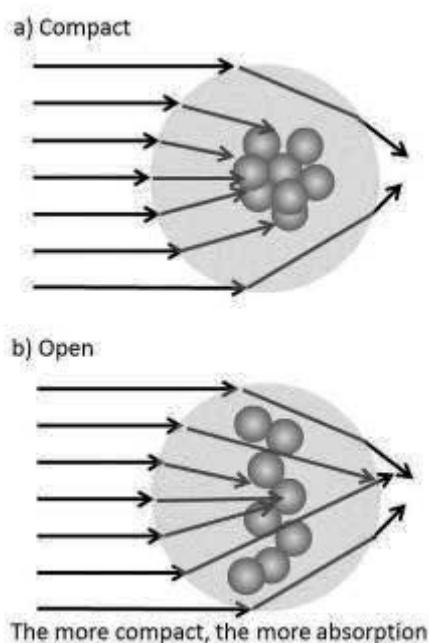
Figure 3 Schematic diagram of the soot shape effect. a) Compacted soot (high fractal dimension) and b) uncompacted soot (low fractal dimension).

Particle shape, that is, the degree of compaction, also affects absorption. Light absorption by a spherical soot particle depends on the particle size and the light wavelength. Light with a wavelength of 550 nm is efficiently absorbed by soot particles ~100 to 200 nm in diameter. Compacted soot has an apparent size within this range. When it is un-

compacted, its apparent size is almost the same as that of the primary particles composing the soot, ~50 nm, and it does not absorb light efficiently.

3.2. Hygroscopic aerosol particles

Hygroscopic aerosol particles change their shape depending on the ambient relative humidity (RH); thus, changes in RH can increase or decrease the light scattering by the particles. An environmental TEM (ETEM) system, by controlling RH, can measure these shape changes, and then their shapes can be used determine the light scattering by the particles. Because particles change their shape and size after deliquescence, the scattering is different from that estimated by Mie theory [4, 5].

4. Summary

Particle shapes vary depending on the sampling location and time and RH. As a result, light scattering and absorption by particles will be increased or decreased compared with that determined by assuming a simple spherical model. Thus, particle shape needs to be considered by climate models.

1 Adachi, K., S. H. Chung and P. R. Buseck, 2010: Shapes of soot aerosol particles and implications for their effects on climate, *J. Geophys. Res.*, **115**, D15206.
2 Bond, T. C., G. Habib and R. W. Bergstrom, 2006: Limitations in the enhancement of visible light absorption due to mixing state, *J. Geophys. Res.*, **111**, D20211, doi: 10.1029/2006JD007315.
3 Fuller, K. A., W. C. Malm and S. M. Kreidenweis, 1999: Effects of mixing on extinction by carbonaceous particles, *J. Geophys. Res.*, **104**, 15,941–15,954.
4 Adachi, K., E. Freney and P. R. Buseck, 2011: shapes of internally mixed hygroscopic aerosol particles after deliquescence, and their effect on light scattering, *Geophys. Res. Let.*, **38**, L13804.
5 Freney, E., K. Adachi, and P. R. Buseck, 2010: Internally mixed atmospheric aerosol particles: Hygroscopic growth and light scattering, *J. Geophys. Res.*, **115**.

Internal mixtures of diesel nanoparticles investigated by FIB-SIMS microscopy

Yuji Fujitani[1,*], Tetsuo Sakamoto[2] and Kentaro Misawa[3]

[1]National Institute for Environmental Studies, 16-2 Onogawa, Tsukuba, Ibaraki 305-8506, Japan
[2]Kogakuin University, 2665-1 Nakanocho, Hachioji, Tokyo 192-0015, Japan
[3]Tokyo Institute of Technology, 4259 Nagatsuta-cho, Midori-ku, Yokohama, Kanagawa 226-8503, Japan

*Corresponding author. Tel.: +81 29 850 2014; Fax: +81 29 850 2014, Email address: fujitani.yuji@nies.go.jp
 (Y. Fujitani)

Information about the physicochemical properties of particles composed of internal mixtures of inorganic and organic materials is necessary to predict particle fate after deposition in the lung and to assess particle toxicity. To measure internal mixtures of inorganic and organic materials in diesel exhaust nanoparticles, we applied a scanning electron microscopy technique, in which Ga-focused ion beam-secondary ion mass spectrometry (FIB-SIMS) is coupled with laser ionization, for observation of diesel particles. We collected particles, generated by an engine operating under no-torque conditions, with aerodynamic diameters of 100–630 nm (subdivided into four size fractions) and with mobility diameters of 30, 50, and 100 nm. By using FIB-SIMS observations, we classified the particles into seven types according to their physical size and chemical composition.

Keywords: Nanoparticle; Ultrafine particle; FIB-SIMS; Imaging; Laser ionization

1. Introduction

Particles, especially insoluble and ultrafine particles (diameter < 100 nm), deposited in the human alveoli are thought to penetrate the cell membrane and enter the bloodstream to be transported to other organs [1, 2]. The adverse health effects due to such insoluble nanoparticles may depend on their chemical composition and shape, as well as on the dose received (number and surface area of the particles). In contrast, the adverse health effects of soluble nanoparticles may depend primarily on their chemical composition and the dose. Thus, the physicochemical properties of nanoparticles, including internal mixtures of inorganic and organic materials, need to be known to predict the toxicity and likely fates of particles after deposition in the lung. Particle fate depends on its solubility in the lung fluid, which in turns depends the particle's composition and how the components are mixed.

In this study, we applied a scanning electron microscopy technique, in which ion beam-secondary ion mass spectrometry (FIB-SIMS) to measure the internal mixture of inorganic and organic materials in diesel exhaust particles and nanoparticles.

2. Methods

An apparatus consisting of a scanning electron microscope and a focused ion beam secondary ion mass spectrometer [3] was used to measure the internal mixture of inorganic and organic material in diesel exhaust nanoparticles. A gallium liquid metal ion source (^{69}Ga and ^{71}Ga mixture) was used for the FIB. Resonance enhanced multi-photon ionization was used for the detection of organic species. Image resolution of up to 50 nm was achieved. Particle morphology was also observed by transmission electron microscopy (TEM; JEM-2010, JEOL).

An 8-L diesel engine (1997 emission regulations) that was not fitted with any after-treatment devices in the Nanoparticle Health Effect Laboratory, National Institute for Environmental Studies [4], was used to generate diesel exhaust particles. The engine was operated at a steady state of 2000 rpm and 0 Nm. Low-sulfur diesel fuel (JIS No. 2 light oil, available and generally used in Japan) and lubricant oil (E Pro Extra 10W-30, Hino) were used. The exhaust was introduced into a primary dilution tunnel and diluted with particle-free clean air with a dilution ratio of about 10 times.

Particles were collected in a size-resolved manner because the depositional area after inhalation is a function of the particle aerodynamic diameter or diffusive equivalent diameter [5], not the physical particle size. Size-resolved particles (aerodynamic diameter, D_{ae} = 100–630 nm, divided into four size fractions) were collected on a silicon wafer by a low-pressure impactor (DLPI, Dekati) in the primary

dilution tunnel. The sample flow rate was 10 L min^{-1} and the sampling duration depended on the targeted size fraction, because particle number concentrations differ according to the size fraction and the particles collected on the silicon wafer in the microscope were required not to overlap. Particles smaller than 100 nm are likely to overlap on the impaction plate because of their high number concentration; therefore, we used a differential mobility analyzer (DMA) and electrical precipitator to distribute the sample evenly on the silicon wafer. Particles with a mobility diameter (D_m) of 30, 50, and 100 nm were collected on the silicon wafer or on collodion membrane-coated copper grids with an electrical precipitator operated at 9 kV after passing through the DMA (SIBATA) with a sheath flow rate of 24 L min^{-1} and a sample flow rate of 2.4 L min^{-1}. The aerodynamic diameter and electrical mobility diameter were equivalent, as shown by the mass size distribution determined by DLPI measurement and the volume size distribution determined by a scanning mobility particle sizer (3034, TSI), in the primary dilution tunnel during sampling. Therefore, we considered there to be no systematic difference between particles >100 nm and <100 nm obtained by the different sampling methods.

3. Results and discussion

Three kinds of physical particles were detected as having D_{ae} = 100–630 nm for each size fraction: agglomerated particles a few micrometers in diameter, oily spot, and smaller particles with a diameter similar to their D_{ae}. Agglomerated particles were apparently soot particles; clusters of ions (C_3, C_4, C_5, C_6), detecting mainly of elemental carbon, were detected. Further, their surface seemed to be coated with an oily substance, because they suddenly shrank when exposed to FIB irradiation. Ca and carbon were detected in the oily spots, indicating that oil mist particle is derived from lubricant oil (Figure 1). The smaller particles consisted mainly of Ca and Cl (Figure 1), or they corresponded to oxidized particles containing Na and K. Carbonaceous particles were also detected without Na or K. We classified the particles with D_{ae} = 100–630 nm into five types according to their physical size and chemical composition. TEM observation indicated that the number of primary particles (about 10 nm) increased as the particle size increased (Figure 2). FIB-SIMS observation showed that particles with D_m = 30–100 nm were of two types, oil mist particles and carbon particles covered with fluorine.

To simulate particle fate after deposition in the lung, the soot particles were exposed to micro mist of acetone generated by electrical spray. FIB-SIMS observation showed that after exposure, the aliphatic hydrocarbons on the soot particle dissolved and dispersed around particle, creating many small particles from the soot particle fragments. From this we infer that after deposition in the alveoli agglomerated particles become disagglomerated in the alveolar lining.

Smaller particles can more easily penetrate the cell membrane and enter the bloodstream, to be transported to other organs. Thus, the fate of these particles after deposition in the lung can be predicted from our data.
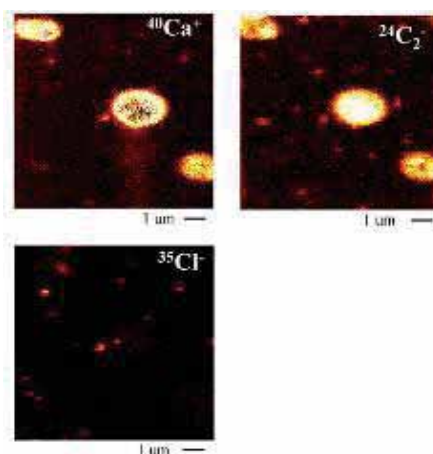
Figure 1 Elemental mapping of Ca$^+$, C$_2^-$, and Cl^{-1} for particles of D_{ae} = 390–630 nm
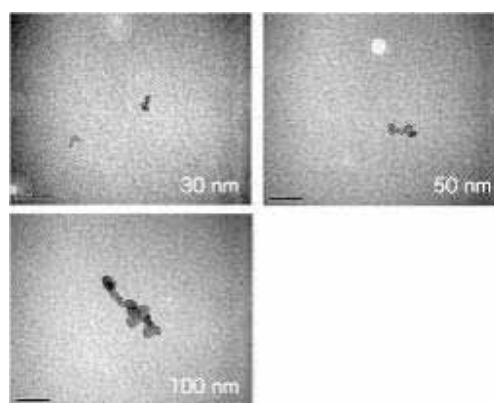
Figure 2 TEM images of particles with D_m = 30, 50, and 100 nm. Scale bar is 100 nm.

1 Takenaka, S., E. Karg, C. Roth, H. Schulz, A. Ziesenis, U. Heinzmann, P. Schramel and J. Heyder, 2001: Pulmonary and systemic distribution of inhaled ultrafine silver particles in rats. *Environ. Health Per.,* **109**,547–551

2 Oberdorster, G., Z. Sharp, V. Atudorei, A. Elder, R. Gelein, A. Lunts, W. Kreyling and C. Cox, 2002: Extrapulmonary translocation of ultrafine carbon particles following whole-body inhalation exposure of rats. *J. Toxicol. Env. Heal. A,* **65**,1,531–1,543

3 Sakamoto, T., M. Koizumi, J. Kawasaki and J. Yamaguchi, 2008: Development of a High Lateral Resolution TOF-SIMS Apparatus for Single Particle Analysis. *Applied Surface Science,* **255**, 1,617-1,620

4 Fujitani, Y., S. Hirano, S. Kobayashi, K. Tanabe, A. Suzuki, A. Furuyama and T. Kobayashi, 2009: Characterization of Dilution Conditions for Diesel Nanoparticle Inhalation Studies. *Inhal Toxicol,* **21**: 200-209

5 ICRP, Human Respiratory Tract Model for Radiological Protection. *ICRP Publication,* 66, Pergamon Press, Oxford.

Modeling atmospheric transport of fine particulate matter with WRF/CMAQ in the Kanto region in summer 2007

Hikari Shimadera[1,*], Hiroshi Hayami[1], Yu Morino[2], Toshimasa Ohara[2], Satoru Chatani[3] and Naoki Kaneyasu[4]

[1]Central Research Institute of Electric Power Industry, 1646 Abiko, Abiko, Chiba 270-1194, Japan
[2]National Institute for Environmental Studies, 16-2 Onogawa, Tsukuba, Ibaraki 305-8506, Japan
[3]Toyota Central R&D Labs., Inc., Nagakute-cho, Aichi-gun, Aichi 480-1192, Japan
[4]National Institute of Advanced Industrial Science and Technology, 16-1 Onogawa, Tsukuba, Ibaraki 305-8569, Japan

*Corresponding author. Tel.: + 81 4 7182 1181; Fax: +81 4 7183 2966, Email address:
simadera@criepi.denken.or.jp (H. Shimadera)

The Community Multiscale Air Quality model was used to analyze atmospheric transport of elemental carbon (EC) and sulfate (SO_4^{2-}) in the Kanto region of Japan in summer 2007. Although the model captured well the long-range transport of EC from the Asian continent, the simulation results indicated that local emissions dominantly contributed to EC concentrations in urban parts of the Kanto region. The model also approximately captured the concentration of SO_4^{2-} and its temporal variation in the region. The simulation results indicated that both domestic emissions in Japan and long-range transport from the Asian continent contribute to SO_4^{2-} concentrations in the Kanto region. When a Pacific high-pressure system covered the Kanto region, local circulation was well developed and consequently domestic emissions, including volcanic emissions, were the dominant contributors, whereas when a high-pressure system prevailed over the East China Sea and low-pressure systems passed north of Japan, synoptic-scale winds associated with this pressure pattern transported large amounts of SO_4^{2-} from the Asian continent to the Kanto region. In addition, although heavy precipitation decreased SO_4^{2-} concentrations near the center of a typhoon, peripheral typhoon winds occasionally played an important role in the long-range transport of SO_4^{2-} from the Asian continent to the Kanto region.

Keywords: $PM_{2.5}$; Air quality model; Sulfate; Elemental carbon; Long-range transport

1. Introduction

Fine particulate matter ($PM_{2.5}$) has several major components, including elemental carbon (EC) and sulfate (SO_4^{2-}). $PM_{2.5}$ has been of increasing concern because it can seriously affect human health. The Ministry of the Environment of Japan established an air quality standard for $PM_{2.5}$ in 2009. Although $PM_{2.5}$ concentrations have decreased in recent years in Japan, the standard for $PM_{2.5}$ is seldom attained in most urban areas. Therefore, better understanding of $PM_{2.5}$ behavior in the atmosphere is required so that measures to attain the standard can be developed.

In this study, the Community Multiscale Air Quality model (CMAQ) [1] driven with meteorological fields produced by the Weather Research and Forecasting model (WRF) [2] was applied to the Kanto region of Japan in summer 2007. In summer, a Pacific high-pressure system often covers Honshu, the main island of Japan. Under this condition, local circulation is well developed and

long-range transport is likely to be of small importance. However, Aikawa et al. (2010: Ref. 3) showed that long-range transport of SO_4^{2-} from the Asian continent contributes importantly to air quality in Japan even in summer. In Japan, summer is also the typhoon season and the heavy precipitation and strong winds associated with typhoons can also affect air quality. The present study analyzed summertime atmospheric transport of EC and SO_4^{2-} in $PM_{2.5}$.

2. Methods

The Advanced Research WRF version 3.2.1 and CMAQ version 4.7.1 were used. The WRF/CMAQ modeling system was run for July and August 2007 with three nested modeling domains, from domain 1, covering a wide area of East Asia, to domain 3, covering most of the Kanto region. Mesoscale and regional-scale objective analysis data of the Japan Meteorological Agency and the final analysis data of the U.S. National Centers for Environmental Prediction

were used for initial and boundary conditions and grid nudging in the WRF simulation. Initial and boundary conditions for the CMAQ simulation were obtained from the Model for Ozone and Related Chemical Tracers version 4 [4]. Emission data were derived from Ohara et al. (2007: Ref. 5) and Zhang et al. (2009: Ref. 6), and estimated by the method described by Chatani et al. (2011: Ref. 7). The CMAQ simulations were conducted for two cases: a baseline simulation case (CB), and a case in which EC and sulfur compound emissions outside Japan and their domain 1 boundary concentrations were set to 0 (CJ).

3. Results and discussion

The simulated EC concentration of CB agreed with the observed black carbon (BC) concentration at the Chichi-Jima Island (about 1000 km south of the center of Tokyo; Figure 1). This result indicates that the model reproduced well the long-range atmospheric transport of EC. It also captured well the temporal variations of EC and SO_4^{2-} concentrations at Komae (about 10 km southwest of the center of Tokyo; Figures 2 and 3). The EC concentration of CB was slightly higher than but similar to that of CJ, indicating that local emissions dominantly contributed to the EC concentration in urban areas of the Kanto region. The differences in the SO_4^{2-} concentrations between CB and CJ indicate that long-range transport from the other countries contributed substantially to SO_4^{2-} concentrations in the Kanto region even in summer. On 15 July, heavy precipitation associated with typhoon 0704 Man-Yi decreased the SO_4^{2-} concentration. On 20 July, the typhoon and the low-pressure system that succeeded it transported EC from the Yellow Sea coastal area to the Chichi-Jima Island, and a volcanic plume from the Miyake-Jima Island increased the SO_4^{2-} concentration at Komae. During 26–29 July and 25–28 August, a high-pressure system prevailed over the East China Sea and low-pressure systems passed north of Japan. Under this typical summertime pressure pattern, the associated synoptic-scale winds transported large amounts of SO_4^{2-} from the Yellow Sea coastal area to Japan. From 31 July to 5 August, peripheral winds of typhoon 0705 USAGI controlled the SO_4^{2-} concentration in the Kanto region by transporting a polluted air mass from the Asian continent and a clean air mass from the Pacific Ocean. After the passage of the typhoon, a Pacific high-pressure system often covered the Kanto region. Under this very typical summer pressure pattern, local sea and land breezes were well developed and the region tended to be less affected by Asian continental outflow. On 21 August, the local circulation accumulated local air pollutants and volcanic gases from Miyake-Jima, and caused high SO_4^{2-} concentrations at Komae.
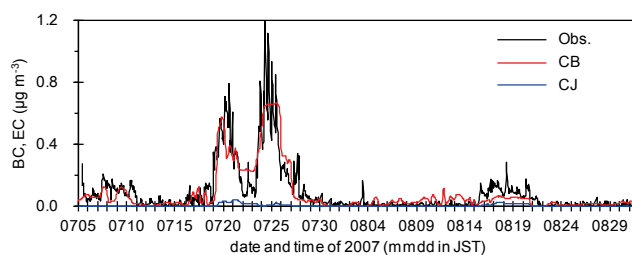
Figure 1 Hourly time series of observed BC and simulated EC concentrations at Chichi-jima.
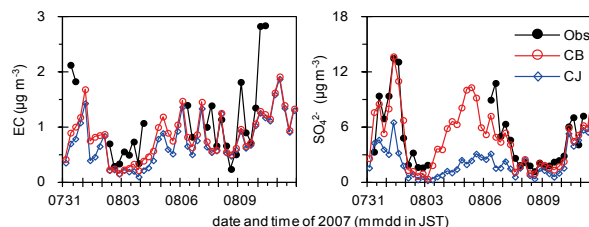
Figure 2 Time series of observed and simulated 6-hour EC and SO_4^{2-} concentrations at Komae.
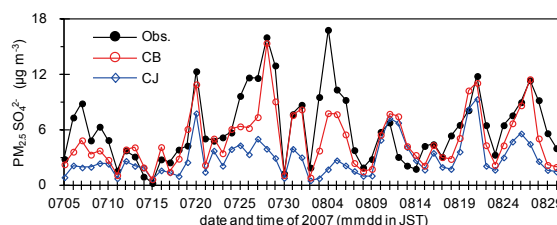
Figure 3 Time series of the observed and simulated daily SO_4^{2-} concentrations at Komae.

1 Byun, D. W. and J. K. S. Ching,1999: Science Algorithms of the EPA Models-3 Community Multi-scale Air Quality (CMAQ) Modeling System. NERL, Research Triangle Park, NC.

2 Skamarock, W. C., J.B. Klemp, J. Dudhia, et al. 2008: A description of the advanced research WRF version 3. NCAR Technical Note, NCAR/TN-475+STR.

3 Aikawa, M., T. Ohara, T. Hiraki, et al. 2010: Significant geographic gradients in particulate sulfate over Japan determined from multiple-site measurements and a chemical transport model: Impacts of transboundary pollution from the *Asian continent. Atmos Environ,* **44**, 381–391

4 Emmons, L K., S. Walters, P. G. Hess, et al. 2010: Description and evaluation of the Model for Ozone and Related chemical Tracers, version 4 (MOZART-4). *Geosci Mod Dev*, **3**, 43–67.

5 Ohara, T., H. Akimoto, J. Kurokawa, et al. 2007: An Asian emission inventory of anthropogenic emission sources for the period 1980-2020. *Atmos Chem Phys*, **7**, 4,419–4,444.

6 Zhang, Q., D. G. Streets, G. R. Carmichael, et al. 2009: Asian emissions in 2006 for the NASA INTEX-B mission. *Atmos Chem Phys,* **9**, 5,131–5,153

7 Chatani, S., T. Morikawa, S. Nakatsuka, et al.2011: Development of a framework for a high-resolution, three-dimensional regional air quality simulation and its application to predicting future air quality over Japan. *Atmos Environ,* **45**, 1,383–1,393

Treatment of black carbon by a global climate model and the potential contribution of electron microscopy

Daisuke Goto[1*], Naga Oshima[2], Teruyuki Nakajima[3] and Toshihiko Takemura[4]

[1]National Institute for Environmental Studies, 16-2 Onogawa, Tsukuba, Ibaraki 305-8506, Japan
[2]Meteorological Research Institute, 1-1 Nagamine, Tsukuba, Ibaraki 305-0052, Japan
[3]Atmosphere and Ocean Research Institute, University of Tokyo, 5-1-5 Kashiwanoha, Kashiwa, Chiba 277-8568, Japan
[4]Research Institute for Applied Mechanics, Kyusyu University, 6-1 Kasuga-koen, Kasuga, Fukuoka 816-8580, Japan

*Corresponding author. Tel.: +81 29 850 2899; fax: +81 29 850 2580, Email address: goto.daisuke@nies.go.jp (D. Goto)

Black carbon (BC) is the most strongly light-absorbing component of aerosols, and the accurate simulation of BC-containing aerosols is required to properly predict aerosol radiative forcing (ARF) and climate change. Different global climate models differently treat categories of BC-containing aerosols and their behaviors in the atmosphere. In this study, we implemented newly parameterized BC aging processes depending on sulfuric acid, BC, and total aerosols into a global three-dimensional aerosol transport–radiation model, SPRINTARS. ARF as predicted by the traditional aging process and a new process differed from that calculated by the original SPRINTARS by about 0.30 Wm^{-2}, a value comparable to the uncertainty suggested by international model in-tercomparison (AeroCom) results.

Keywords: Black carbon (BC); BC Aging process; Global aerosol model; BC radiative forcing

1. Introduction

Black carbon (BC) aerosol particles strongly absorb shortwave radiation and thus influence radiative perturbation more strongly than other aerosol components [1-3]. Estimates of the direct radiative impacts of an aerosol due to BC derived from fossil fuel and biomass burning still include large uncertainty, with positive forcings of +0.20 ± 0.15 and +0.03 ± 0.12 W m^{-2}, respectively [3]. The uncertainty of the BC radiative effects may reflect uncertainties in both the spatial distribution of BC, which depends on various atmospheric processes such as emission, transport, chemical transposition (BC aging), and deposition processes [4-7], and BC optical properties [8]. Among general circulation models (GCMs) and models included in the Aero-Com model intercomparison project, differences in the BC aging process are large (Table 1). Most aerosol climate models still use parameterization to simplify the BC aging process.

Therefore, in this study, we investigated how differences in the treatment of the BC aging process affected the BC spatial distribution and thus BC radiative forcing. For this purpose, we performed numerical experiments with SPRINTARS, a global aerosol transport–radiation model [9-13], which also is a participant in the AeroCom project, using three different types of treatment for BC aging processes: (1) the original SPRINTARS method (ORIG); (2) the traditional method, which uses a constant aging time-scale with e-fold lifetime (τBC) through coagulation and condensation and is widely used in global models (AGF); (3) a method similar to AGF but using a variable τBC value that is calculated online by a new parameterization of BC aerosols based on a spectral-binning method (AGV) [14].

Table 1 Summary of BC aging processes used in global models

Name[a]	Method[b]	Time scale of BC aging[c]	Computer cost[d]
UMI	None	Zero (No aging)	---
UIO_CTM	Param.	Const.	Light
LOA	Param.	Const.	Light
LSCE	Param.	Const.	Light
MPI_HAM	Explicit	Var.	Heavy
GISS	Param.	Const.	Light
UIO_GCM	Explicit	Var.	Heavy
SPRINTARS	Param.	Zero[e]	Light
ULAQ	Param.	Const.	Light
GOCART	Param.	Const.	Light

[a] Model name as shown in the AeroCom project [4]
[b] Param., parameterization; Explicit, explicit expression
[c] Zero, no decay; Const., constant timescale of decay; Var., variable timescale of decay
[d] CPU time required to calculate the process
[e] See section 2

2. Methods

2.1. Global aerosol radiation model (SPRINTARS)

We implemented three different BC aging processes in a global three-dimensional aerosol transport-radiation model, the Spectral Radiation-Transport Model for Aerosol Species (SPRINTARS) [9-13, 15, 16]. SPRINTARS has been implemented within an atmospheric GCM developed by the former Center for Climate System Research (now Atmosphere and Ocean Research Institute) of the University of Tokyo, National Institute for Environmental Studies, and the Frontier Research Center for Global Change, and used for climate modeling [17]. The model has also been implemented within a radiation scheme called MSTRN-8 [18, 19]. SPRINTARS calculates the mass mixing ratios of the main tropospheric aerosols, namely, carbonaceous aerosols, including water-soluble BC (WSBC), water-insoluble BC (WIBC), and organic particles (OC); sulfate, soil dust, sea salt, and the precursor gases of sulfate (SO_2 and dimethyl sulfide). SPRINTARS considers atmospheric processes, including emission, advection, diffusion, sulfur chemistry, deposition, and gravitational settling. We used emission inventories and nudging conditions described previously [10, 15]. The spatial and vertical resolutions were set to T42 (i.e., $2.8° \times 2.8°$ horizontally and 20 vertical layers).

2.2. Treatment of BC

The three ways of treating BC aging processes implemented in SPRINTARS are shown schematically in Figure 1.
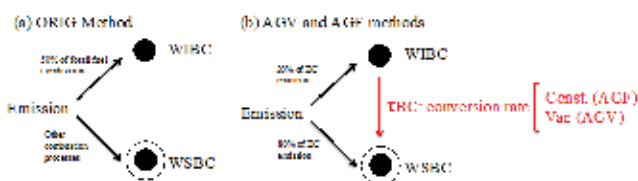
Figure 1 Schematic diagram of the three BC aging processes implemented.

2.2.1. Original method (ORIG)

In ORIG, WIBC is not converted to WSBC; that is, it is assumed that no BC aging occurs in the atmosphere. BC aerosols are categorized into three types: pure BC (i.e., WIBC) and two types of WSBC (BC/OC = 6.67 or 3.33). In the original SPRINTARS, the partitioning ratio of WSBC into each mode is diagnosed by the fractions of WSBC and OC in one grid cell of the GCM. Therefore, ORIG treats three carbonaceous tracers: OC, WSBC, and WIBC. In ORIG, half of the BC emitted by fossil fuel combustion is assumed to be externally mixed with other species (i.e., WIBC), whereas the BC from biomass burning, agricultural activities, and biofuel combustion is considered to become internally mixed with OC (i.e., WSBC) within one time step (about 20 min) of the GCM in one grid cell (about 300 km by 300 km).

2.2.2. AGV and AGF

In AGV and AGF, BC aging in the atmosphere is expressed by the conversion timescale with e-fold lifetime, τBC, from WIBC to WSBC. The change in WIBC in time t can be expressed in terms of τBC as follows:

$$[WIBC](t) = [WIBC](t-1) + [WIBC](t-1) \times \exp(-t/\tau BC),$$
(1)
$$[WSBC](t) = [WSBC](t-1) - [WIBC](t-1) \times \exp(-t/\tau BC),$$
(2)

where [WIBC] and [WSBC] are the concentrations of WIBC and WSBC, respectively. In AGF the τBC value is generally fixed at 1 to 1.2 days (see section 1) [20, 21]. In AGV, however, τBC is allowed to vary, depending on the number concentration of the particles to be aged and the concentrations of condensed gases. In this method, we used a new parameterization of τBC that takes into account the dependence of the aging process on various conditions. This parameterization was developed by Liu et al. [5], who used a detailed physics-based aerosol mixing state-resolved box model for the purpose [22, 23]. However, this parameterization only addresses the growth of BC by condensation, and ignores other BC aging processes (e.g., by coagulation). Therefore, we set the maximum τBC to 20 days following [7].

3. Results

We compared three methods using the horizontal distribution of the annually averaged BC mass concentration at the surface (Figure 2). We found that the difference in the calculated BC mass concentration among the three methods was at most 10% near aerosol sources and at most 50% over remote areas (Figures 2b and 2c). The differences among the methods near aerosol source regions such as North America exceeded the differences between the simulations and the observations (not shown). Therefore, these differences may reflect mainly the uncertainty of the BC emission inventory.

We also compared the annually averaged ratio of WIBC to total BC (WIBC + WSBC) (hereafter, the WIBC ratio) at the surface with that at the sigma 0.5 level (Figure 3). In ORIG, the WIBC ratio at the surface ranged from 10% to 30% over the BC source regions (United States, Europe, China, and India) and were smaller over oceans (from 30% to 40%), because the WIBC particles, which are inefficiently removed by rainout during precipitation events, do not age in ORIG but remain in the atmosphere, whereas WSBC particles are efficiently removed. In contrast, in both AGF and AGV, the WIBC ratios at the surface over most land areas become much larger than those over oceans. In AGV, the WIBC ratios are larger than those in AGF over most of the world, because the magnitude of the conversion timescale is smaller in AGV than in AGF. As a result,

WIBC ages more rapidly in AGF than in AGV and more is scavenged by wet deposition. Therefore, the contrast in the WIBC ratio between land and ocean in ORIG is very different from that in both AGV and AGF. Theoretically, the WIBC ratio tends to be higher over BC source regions (land) than over outflow regions (ocean), because the amount of BC that is aged by condensation of gases or other aerosols is in proportion to the amount of time the BC particles remain suspended in the atmosphere [24-27].
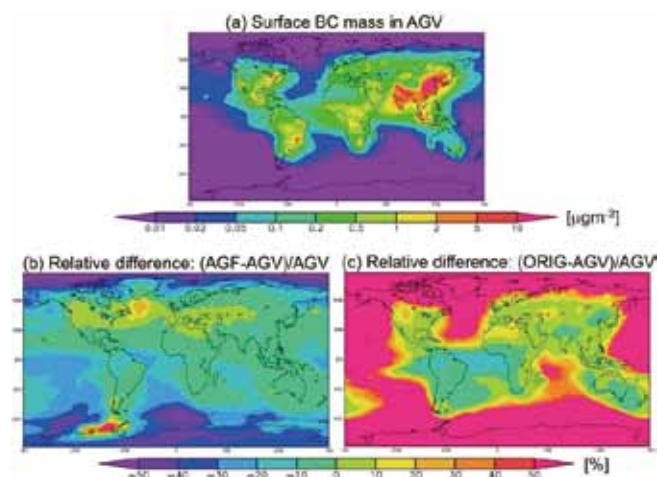
Figure 2 Global distributions of annually averaged (a) surface BC mass concentrations obtained by the AGV method, and the relative differences in BC mass concentrations (b) between AGF and AGV and (c) between ORIG and AGV.
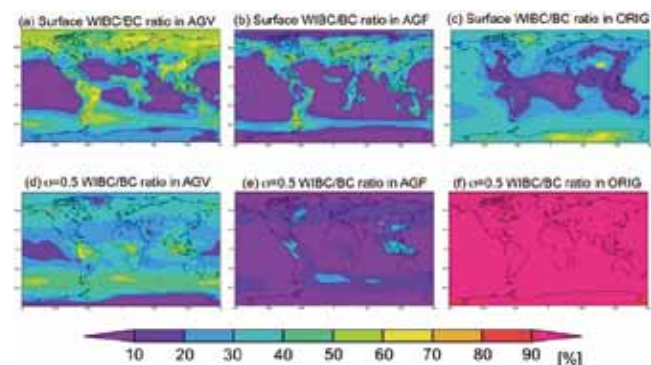
Figure 3 Annual mean ratio of WIBC to total BC at the surface and at the sigma 0.5 level.

These differences in the WSBC ratio among the methods result in differences in the absorption aerosol optical thickness (AAOT) (Figure 4). The AAOT values in AGV tend to be larger than those in the other two methods, especially over biomass burning regions. This difference can be explained in part by the gap in AAOT between simulation and observation [4].
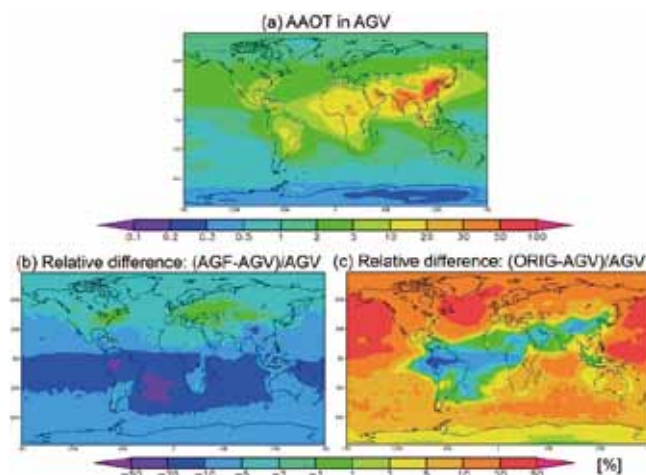
Figure 4 Global distribution of annually averaged (a) AAOT obtained by the AGV method and the relative differences in AAOT (b) between AGF and AGV and (c) between ORIG and AGV.

Finally, we estimated aerosol radiative forcing caused by the aerosol direct effect due to anthropogenic BC to be +0.300 Wm^{-2} (AGV), +0.047 Wm^{-2} (AGF), and +0.356 Wm^{-2} (ORIG). Thus, AGF tended to underestimate the amount of aerosol light absorption compared with the other methods (AGV and ORIG).

4. Conclusions

Differences in the treatment of BC aging in aerosol modeling studies can cause differences of up to about 0.3 Wm^{-2} in the aerosol radiative forcing due to BC. This value is comparable to the uncertainty suggested by AeroCom results. Therefore, this problem needs to be addressed further by obtaining new information from field measurements and in situ experiments. In this regard, electron microscopy could contribute to global modeling by providing microphysical information, for example, the fraction of BC-containing particles relative to total atmospheric particles and the proportion of BC in BC-containing particles.

1 Hansen, J., M. Sato and R. Ruedy, 1997: Radiative forcing and climate response, *J. Geophys. Res.*, **102**, D6, 6,831-6,864.
2 Jacobson, M. Z., 2002: Control of fossil-fuel particulate black carbon and organic matter possibly the most effective method of slowing global warming, *J. Geophys. Res.*, **107**(D19), 4,410, doi: 10.1029/2001JD001376.
3 Forster, P., V. Ramaswamy, P. Artaxo, T. Berntsen, R. Betts, D. W. Fahey, J. Haywood, J. Lean, D. C. Lowe, G. Myhre, J. Nganga, R. Prinn, G. Raga, M. Schulz and R. Van Dorland, 2007: Changes in Atmospheric

Constituents and in Radiative Forcing. In: Climate Change 2007: The Physical Science Basis. Contribution of Working Group I to the Fourth Assessment Report of the Intergovernmental Panel on Climate Change (Solomon, S. et al. (eds.). Cambridge University Press, Cambridge, United Kingdom and New York, NY, USA.

4 Koch, D., M. Schulz, S. Kinne, C. McNaughton, J. R. Spackman, Y. Balkanski, S. Bauer, T. Berntsen, T. C. Bond, O. Boucher, M. Chin, A. Clarke, N. De Luca, F. Dentener, T. Diehl, O. Dubovik, R. Easter, D. W. Farey, J. Feichter, D. Fillmore, S. Freitag, S. Ghan, P. Ginoux, S. Gong, L. Horowitz, T. Iversen, A. Kirkevåg, Z. Klimont, Y. Kondo, M. Krol, X. Liu, R. Miller, V. Montanaro, N. Moteki, G. Myhre, J. E. Penner, J. Perlwitz, G. Pitari, S. Reddy, L. Sahu, H. Sakamoto, G. Schuster, J. P. Schwarz, Ø. Seland, P. Stier, N. Takegawa, T. Takemura, C. Textor, J. A. van Aardenne and Y. Zhao, 2009: Evaluation of black carbon estimations in global aerosol models. *Atmos. Chem. Phys.*, **9**, 9,001-9,026.

5 Liu, J. F., S. M. Fan, L. W. Horoqitz and H. Levy II, 2011: Evaluation of factors controlling long-range transport of black carbon to the Arctic, *J. Geophys. Res.*, **116**, D04307, doi: 10.1029/2010JD015145.

6 Schulz, M., C. Textor, S. Kinne, Y. Balkanski, S. Bauer, T. Bertsen, T. Berglen, O. Boucher, F. Dentener, S. Guibert, I. S. A. Isaksen, T. Iversen, D. Koch, A. Kirkevag, X. Liu, V. Montanaro, G. Myhre, J. E. Penner, G. Pitari, S. Reddy, O. Seland, P. Stier and T. Takemura, 2006: Radiative forcing by aerosols as derived from the AeroCom present-day and pre-industrial simulations, *Atmos. Chem, Phys.*, **6**, 5,225-5,246.

7 Shindell, D. T., M. Chin, F. Dentener, R. M. Doherty, G. Faluvegi, A. M. Fiore, P. Hess, D. M. Koch, I. A. MacKenzie, M. G. Sanderson, M. G. Schultz, M. Schulz, D. S. Stevenson, H. Teich, C. Textor, O. Wild, D. J. Bergmann, I. Bey, H. Bian, C. Cuvelier, B. N. Duncan, G. Folberth, L. W. Horowitz, J. Jonson, J. W. Kaminski, E. Marmer, R. Park, K. J. Pringle, S. Schroeder, S. Szopa, T. Takemura, G. Zeng, T. J. Keating and A. Zuber, 2008: A multi-model assessment of pollution transport to the Arctic, *Atmos. Chem. Phys.*, **8**, 5,353-5,372.

8 Bond, T. C. and R. W. Bergstrom, 2006: Light absorption by carbonaceous particles: an investigative review, *Aerosol Science and Tech.*, **40**, 27-67.

9 Goto, D., T. Takemura and T. Nakajima, 2008: Importance of global aerosol modeling including secondary organic aerosol formed from monoterpene, *J. Geophys. Res.*, **113**, D07205, doi: 10.1029/2007JD009019.

10 Goto, D., T. Nakajima, T. Takemura and K. Sudo, 2011: A study of uncertainties in the sulfate distribution and its radiative forcing associated with sulfur chemistry in a global aerosol model. *Atmos. Chem. Phys.*, **11**, 10,889-10,910.

11 Takemura, T., H. Okamoto, Y. Maruyama, A. Numaguti, A. Higurashi and T. Nakajima, 2000: Global three-dimensional simulation of aerosol optical thickness distribution of various origins, *J. Geophys. Res.*, **105**, 17,853–17,873.

12 Takemura, T., T. Nakajima, O. Dubovik, B. N. Holben and S. Kinne, 2002: Single scattering albedo and radiative forcing of various aerosol species with a global three-dimensional model, *J. Climate*, **15**, 333–352.

13 Takemura, T., T. Nozawa, S. Emori, T. Y. Nakajima and T. Nakajima, 2005: Simulation of climate response to aerosol direct and indirect effects with aerosol transport-radiation model, *J. Geophys. Res.*, **110**, D02202, doi: 10.1029/2004JD005029.

14 Oshima, N. and M. Koike, 2012: Development of a parameterization of black carbon aging for use in general circulation models, *Geo. Model Dev. Discuss*, **5**, 1,263-1,293.

15 Goto, D., N. A. J. Schutgens, T. Nakajima and T. Takemura, 2011: Sensitivity of aerosol to assumed optical properties over Asia using a global aerosol model and AERONET, *Geophys. Res., Lett.*, **38**, L17810, doi: 10.1029/20011GL048675.

16 Goto, D., T. Takemura, T. Nakajima and K. V. S. Badarinath, 2011: Global aerosol model-derived black carbon concentration and single scattering albedo over Indian region and its comparison with ground observations, *Atmos. Environ.*, **45**, 3,277-3,285.

17 Hasumi, H. and S. Emori, 2004: K-1 Model Developers: K-1 coupled GCM (MIROC) description, *K-1 Tech. Rep.* **1**, Univ. of Tokyo, Tokyo.

18 Nakajima, T., M. Tsukamoto, Y. Tsushima, A. Numaguti and T. Kimura, 2000: Modeling of the radiative process in an atmospheric general circulation model, *Appl. Opt.*, **39**, 4,869–4,878

19 Sekiguchi, M. and T. Nakajima 2008: A k-distribution-based radiation code and its computational optimization for an atmospheric general circulation model. *J. Quant. Spectrosc. Radiat. Transfer*, **109**, 2,779-2,793.

20 Chin, M., P. Ginoux, S. Kinne, O. Torres, B. N. Holben, B. N. Duncan, R. V. Martin, J. A. Logan, A. Higurashi and T. Nakajima, 2002: Tropospheric aerosol optical thickness from the GOCART model and comparisons with satellite and sun photometer measurements, *J. Atmos. Sci.,* **59**, 461-483

21 Chung, S. H. and J. H. Seinfeld, 2002: Global distribution and climate forcing of carbonaceous aerosols, *J. Geophys. Res.*, **107**(D19), 4407, doi: 10.1029/2001JD001397.

22 Oshima, N., M. Koike, Y. Zhang, Y. Kondo, N. Moteki, N. Takegawa and Y. Miyazaki, 2009: Aging of black carbon in outflow from anthropogenic sources using a mixing state resolved model: Model development and evaluation, *J. Geophys. Res.*, **114**, D06210, doi: 10.1029/2008JD010680.

23 Oshima, N., M. Koike, Y. Zhang and Y. Kondo, 2009: Aging of black carbon in outflow from anthropogenic sources using a mixing state resolved model: 2. Aerosol optical properties and cloud condensation nuclei activities, *J. Geophys. Res.*, **114**, D18202, doi: 10.1029/2008JD011681.

24 Moteki, N., Y. Kondo, Y. Miyazaki, N. Takegawa, Y. Komazaki, G. Kurata, T. Shirai, D. R. Blake, T. Miyakawa and M. Koike, 2007: Evolution of mixing state of black carbon particles: Aircraft measurements over the western Pacific in March 2004, *Geophys. Res., Lett.*, **34**, L11803, doi: 10.1029/2006GL028943.

25 Clarke, A. D., Y. Shinozuka, V. N. Kapustin, S. Howell, B. Huebert, S. Doherty, T. Anderson, D. Covert, J. Anderson, X. Hua, K. G. Moore II, C. McNaughton, G. Carmichael and R. Weber, 2004: Size distributions and mixtures of dust and black carbon aerosol in Asian outflow: Physiochemistry and optical properties, *J. Geophys. Res.*, **109**, D15S09, doi: 10.1029/2003JD004378

26 Schwarz, J. P., R. S. Gao, D. W. Fahey, D. S. Thomson, L. A. Watts, J. C. Wilson, J. M. Reeves, M. Darbeheshti, D. G. Baumgardner, G. L. Kok, S. H. Chung, M. Schulz, J. Hendricks, A. Lauer, B. Kärcher, J. G. Slowik, K. H. Rosenlof, T. L. Thompson, A. O. Langford, M. Loewenstein and K. C. Aikin, 2006: Single-particle measurements of midlatitude black carbon and light-scattering aerosols from the boundary layer to the lower stratosphere, *J Geophys. Res.*, **111**, D16207, doi: 10.1029/2006JD007076.

27 Shiraiwa, M., Y. Kondo, N. Moteki, N. Takegawa, Y. Miyazaki and D. R. Blake, 2007: Evolution of mixing state of black carbon in polluted air from Tokyo, *Geophys. Res. Lett.*, **34**, L16803, doi: 10.1029/2007GL029819.

Aerosol particle analysis with INCAFeature TEM

Chizu Mitsui[1*], Chieko Hamamoto[2] and Hideo Nishioka[2]

[1]Oxford Instruments KK, 2-11-6, Tomioka, Koto-ku, Tokyo 135-0047, Japan
[2]JEOL Ltd., 3-1-2 Musashino, Akishima, Tokyo 196-8558, Japan

*Corresponding author. Tel.: +81 3 5245 3591; Fax: +81 3 5245 4477, Email address: chizu.mitsui@oxinst.com (C. Mitsui)

Energy dispersive X-ray spectroscopy (EDS) is an established technique used to characterize the elemental composition of a sample under the beam of an electron microscope. INCAFeature is an automated feature detection and analysis system in which an electron microscope is used for feature detection and EDS is used to determine the chemistry of each feature. Although a particle analysis with an scanning electron microscopy-EDS system is often used for non-metallic inclusions in steel or gunshot residue, few studies have used a transmission electron microscopy (TEM)-EDS system because of sample size and focusing difficulties. In this study, we conducted a first trial of automated particle analysis with a TEM-EDS system and succeeded in automatically detecting and analyzing 158 particles in just 31 min. By automating labor-intensive statistical calculations, INCAFeature can accelerate the progress of aerosol studies.

Keywords: Aerosol particles; Energy dispersive X-ray spectroscopy; Elemental composition; Automated analysis; Particle analysis; Electron microscopy

1. Introduction

Energy dispersive X-ray spectroscopy (EDS) is an established technique used to characterize the elemental composition of a sample under the beam of an electron microscope. INCAFeature is an automated particle detection and analysis system that uses electron microscopy for feature detection and EDS for determining the chemistry of each particle. Although a scanning electron microscopy-EDS system is often used for particle analysis of non-metallic inclusions in steel or gunshot residue, few studies have used a transmission electron microscopy (TEM)-EDS system because of sample size and focusing difficulties. In this study, we conducted a first trial of automated particle analysis with a TEM-EDS system.

2. Instrument configuration

EDS system: INCAFeature, a particle detection and identification system
EDS detector: X-MAXTEM, 80 mm^2 (Oxford Instruments Ltd.)
TEM: JEM-1400 (JEOL Ltd.)

3. Aerosol particles

An aerosol is a colloid suspension of fine particles in a gas. Aerosols scatter and absorb solar and terrestrial radiation. Moreover, by forming clouds, they influence climate and meteorology. Aerosol particles have complex chemical compositions and vary over a wide size range, depending on their origin and on atmospheric processes. The number, size and chemical composition of aerosol particles have important consequences for meteorological phenomena. In this study, aerosol particles were applied to a carbon filter for TEM imaging and EDS analysis.

4. Results

On a TEM image (Figure 1), aerosol particles appear as small dark particles and brighter amorphous features. The dark particles are composed mainly of carbon, silicon, and some metals (data not shown), whereas the brighter particles are sulfate.

Gray-level thresholding of the image is used to identify the gray particles on the filter. Figure 2 shows aerosol particles imaged by TEM and scanning TEM (STEM; dark-field), and detected by INCAFeature. Sulfate particles are brighter than the filter used to obtain the STEM image. Detected particles were colored individually.
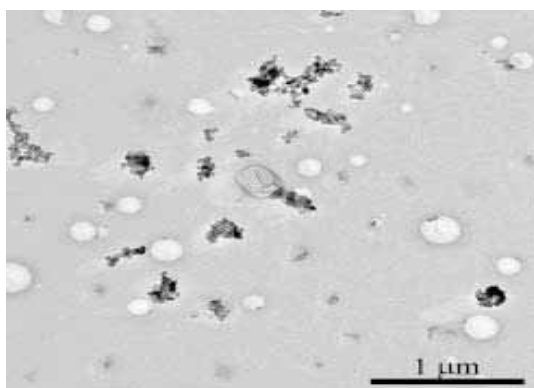
Figure 1 TEM image of aerosol particles applied to a carbon film.
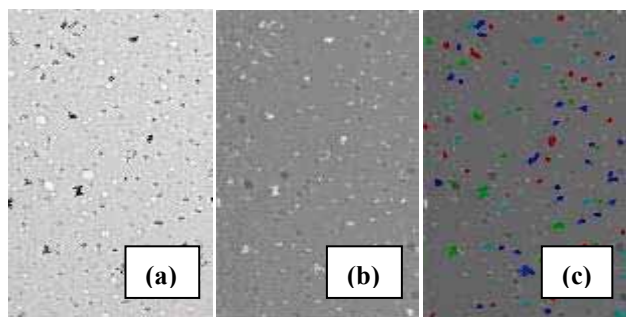
Figure 2 Aerosol particles imaged by (a) TEM and (b) STEM (dark-field) and (c) detected by using INCAFeature
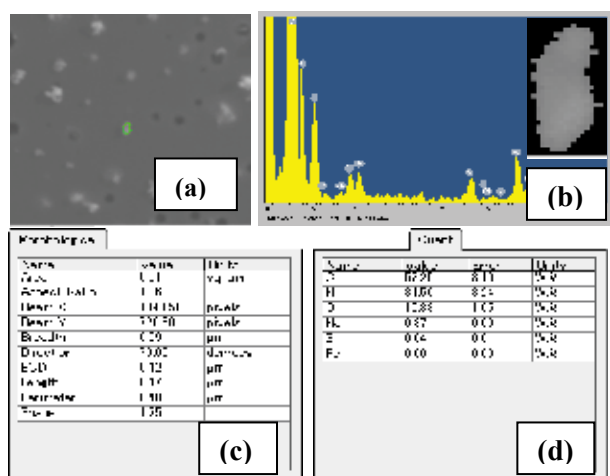
Figure 3 INCAFeature TEM results for a single particle: (a) STEM image, (b) binary image and X-ray spectrum, and information on the particle's (c) morphology and (d) chemistry.

To acquire a STEM image for morphological measurement, all detected particles were scanned again; the electron beam scanned each particle continuously and its X-ray spectrum was determined with the EDS detection system. The automated analysis of a particle by INCA Feature produces a STEM image of the particle and its X-ray spectrum, and

information on its morphology and chemical composition (Figure 3). Then, the particle is classified on the basis of its morphology and chemistry (Figure 4).

In this trial, 158 particles were detected automatically in a 12 μm × 12 μm area, and particle detection and measurement took just 31 min. The automated statistical data processing can be performed using the particle chemistry or its morphology, or a combination of the two (Figures 5 and 6).

Figure 4 Example of particle data. Scatter plot of area vs perimeter (left), and a quant bar summarizing all of the elements and their concentrations (right)

Classe	Number of particles	% of total particles	Particle area (sq um)	% of total area
Includes S, Aspect ratio 1~1.5	70	44.3	1.63E+00	1.146
Includes S, Aspect ratio 1.5~2	68	38.0	1.67E+00	1.178
Includes S, Aspect ratio 2~	20	12.7	5.63E+01	0.398

Figure 5 Example statistical analyses
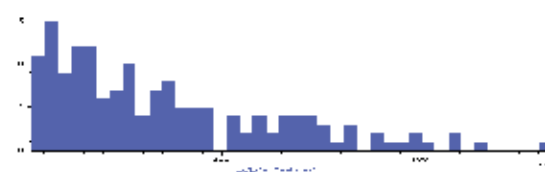
Figure 6 Histogram showing the frequency distribution of one morphological measurement. Most particles were smaller than 200 μm equivalent circle diameter (ECD).

5. Conclusion

INCAFeature, an automated particle analyzing system used in conjunction with TEM, is a powerful tool for aerosol studies. Typically, particle analysis by TEM-EDS is done manually point by point, which requires an immense amount of time and effort. With INCAFeature, we succeeded in automatically detecting and analyzing 158 particles in just 31 min, and data processing was done in parallel. Thus, by automating labor-intensive statistical processing, INCA Feature can further the progress of aerosol studies.

Aerosol isotope analysis by secondary ion mass spectrometry

Masashi Nojima

1Research Institute of Science and Technology, Tokyo University of Science, 2461 Yamazaki, Noda-shi, Chiba 278-8510, Japan

*Corresponding author. Tel.: +81 4 7124 1501 (Ext. 5025), Email address: mnojima@rs.noda.tus.ac.jp (M. Nojima)

This study focuses on radioisotopes on aerosols exposed to radionuclides produced by the Fukushima Daiichi nuclear disaster. Radioisotopes are transported by wind in the gas phase or adsorbed onto aerosol particles. The distribution of radioisotopes in the environment depends on the aerosol particle size and the radionuclides present, factors that must be considered when investigating the areas polluted by radioisotopes and internal contamination in our bodies. In this study, size-classified aerosol particle samples were collected with a cascade impactor and analyzed by secondary ion mass spectrometry.

Keywords: Size-classified analysis; Radioisotope aerosol; Fukushima Daiichi nuclear disaster; SIMS

1. Introduction

This study focused on radioisotopes on aerosols that were exposed to radionuclides produced by the Fukushima Daiichi nuclear disaster. Radioisotopes are carried by winds in gas phase or adsorbed onto aerosol particles. The distribution of radioisotopes in the environment depends on the aerosol particle size and the radionuclides present, and these factors must be considered in investigations of the areas polluted by radioisotopes and internal contamination in our bodies.

Radioactive contamination is frequently discussed only in terms of dose. The objective of this study was to clarify the relationship between radionuclide distribution in the environment and the size of aerosol particles, which is not taken into account by the Japanese System for Prediction of Environmental Emergency Dose Information. In this study, size-classified aerosol particle samples were collected by cascade impactor and analyzed by secondary ion mass spectrometry (SIMS).

2. Methods

Aerosols were sampled with an MCAS-03 aerosol sampler (Murata Inc.) that filtered the particles into three size fractions according to their aerodynamic diameter: >10 μm, 2.5–10 μm, and <2.5 μm.

The sampling locations were Katsuomura, in Fukushima Prefecture, almost 20 km from the Fukushima Daiichi nuclear power plant; Noda, in Chiba Prefecture, which is near a nuclear fallout hot spot; and Aihara, in Tokyo, where the dose measured after the disaster was nearly the same as that before the disaster. In some locations, the aerosol sampler was powered by electricity provided by an AC backup system; MBS-300S-TR1 (Miyauchi works).

The aerosol samples on the sampling plates were introduced into a dynamic SIMS system (IMS-4f; AMETEK, Inc.) and supplied with 4.5 kV of energy. The primary ion beam was O_2^+ (acceleration energy, 10 kV; beam current, 30 nA). In this system, secondary ions generated by a sputtering process are separated by their energy and mass by a mass spectrometer.

3. Estimation of size-classified aerosols

In addition to the SIMS analysis, the size-classified aerosol particles were examined by scanning electron microscopy (SEM) and energy dispersive X-ray spectroscopy (EDX) (Figure 1). In this figure, the SEM images show each size fraction of the aerosol sampled at Noda. Fine aerosol particles (<2.5 μm) are observed on the resin fibers, and an aggregate of aerosol particles of intermediate size . A single aerosol particle of the >10 μm size fraction is also shown.

The mass spectrum of the <2.5 μm aerosol particles shows a strong peak at m/z = 131. The peak may represent radioiodine already transformed by beta decay to ^{131}Xe in the nuclear reactor [1]. The mass spectrum of the aerosol particle > 10 μm in diameter shows two strong peaks at m/z = 139 and 141. These may represent the main fission products of the following nuclear reactions:

$$^{235}U + n \rightarrow \, ^{92}Kr + \, ^{141}Ba + 3n \qquad (1)$$
$$^{235}U + n \rightarrow \, ^{95}Y + \, ^{139}I + 2n \qquad (2)$$
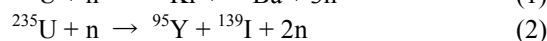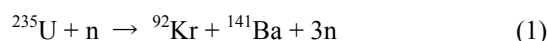
These elements are not stable, and by the time they were released into the atmosphere their decay products were no
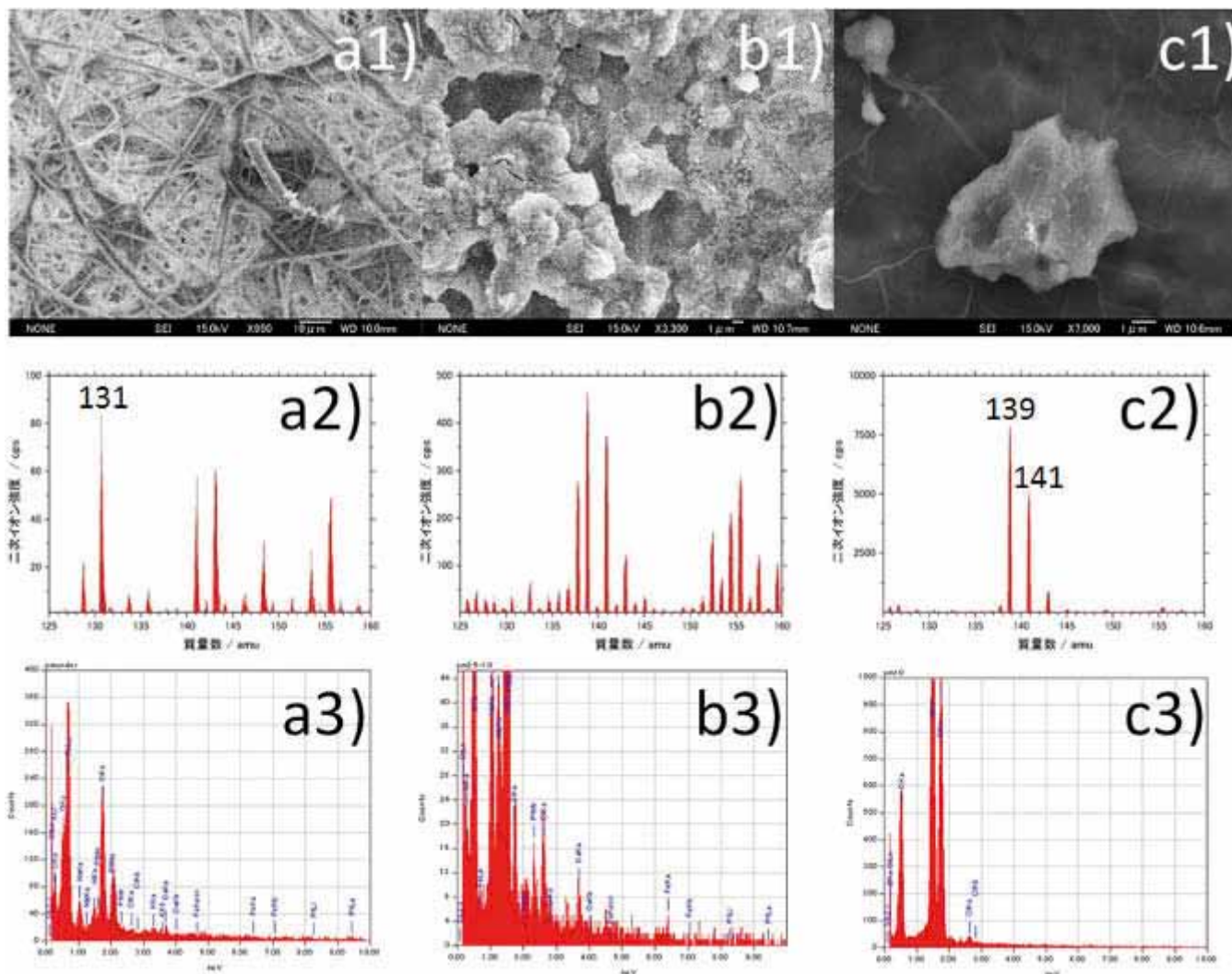
Figure 1 SEM images (top row), mass spectra (middle), and EDX spectra (bottom) of size-classified aerosol particles: a) <2.5 µm; b) 2.5–10 µm; c) >10 µm.

longer radioactive.

The EDX spectra show that the main elements in the sampled aerosol were carbon, oxygen, and silicon. No elements generated by the nuclear disaster were detected. Small particles also included sodium and chlorine, probably from sea salt.

4. Concluding remarks

To clarify the size relationship between aerosol particles and radionuclides, a size-classified aerosol sample was obtained by cascade impactor and analyzed by SIMS.

The mass spectrum of particles < 2.5 µm showed a strong peak at m/z = 131, suggesting radioiodine already trans-formed by beta decay to ^{131}Xe in the nuclear reactor. The mass spectrum of particles > 10 µm showed two peaks (m/z = 139 and 141) that may have originated as the main fission products of the nuclear reactions.

1 Aregbe, Y., K. Mayer, S. Valkiers and P. De Bièvre, 1996: *International Journal of Mass Spectrometry and Ion Processes*, Volume **154**, Issues 1–2, Pages 89–97.

Aging of black carbon and its impact on aerosol optical properties and cloud condensation nuclei activities using a mixing state resolved model

Naga Oshima[*]

[1]Atmospheric Environment and Applied Meteorology Research Department, Meteorological Research Institute, 1-1 Nagamine, Tsukuba, Ibaraki 305-0052, Japan

*Corresponding author. Tel.: +81 29 853 8712; Fax: +81 29 855 7240, Email address: oshima@mri-jma.go.jp (N. Oshima)

   The mixing state of black carbon (BC) aerosols, namely, the degree to which BC particles are coated with other aerosol components, has been recognized as important for evaluating aerosol radiative forcing. In order to resolve the BC mixing state explicitly in model simulations, the Model of Aerosol Dynamics, Reaction, Ionization, and Dissolution with resolution of the mixing state of BC (MADRID-BC) was developed. MADRID-BC uses a two-dimensional (2-D) aerosol representation, in which aerosols are given for individual particle diameters and BC mass fractions, and it can accurately simulate changes in the entire BC mixing state resulting from condensation/evaporation processes. Aircraft observations conducted in March 2004 show that the mass fraction of thickly-coated BC particles increased in air horizontally transported out from an urban area in Japan within the planetary boundary layer (PBL) over the ocean. MADRID-BC generally reproduces this feature well when observed bulk aerosol concentrations are used as constraints. MADRID-BC was applied to evaluate the influence of changes in the BC mixing state on aerosol optical properties and cloud condensation nuclei (CCN) activities in these air parcels. The evaluation shows that coatings on BC particles enhance light absorption at a wavelength of 550 nm by 38% in air leaving the source region, and by 59% after transport over the ocean for half a day. When the model treats aerosols using the conventional size-resolved sectional representation that does not resolve BC mixing states, the simulated absorption coefficients and single scattering albedos are greater by 35–44% and smaller by 7–13%, respectively, than those from a simulation that resolves the BC mixing state. These results indicate that it is essential for atmospheric models to take into account BC-free particles for accurate prediction of aerosol optical properties, because the conventional representation cannot separately treat BC-containing and BC-free particles in each size bin. Moreover, 55% and 83% of BC-containing particles (by BC mass concentration) can act as CCN at a supersaturation of 0.05% when they leave the source region and after transport for half a day, respectively. These results suggest the importance of the uplift of BC particles from the PBL near source regions for their efficient long-range transport in the free troposphere.

Keywords: Aerosol modeling; Black carbon; Mixing state; Aging; Aerosol optical properties; Cloud condensation nuclei

1. Introduction

   Black carbon (BC) aerosols (soot) in the atmosphere efficiently absorb solar radiation and are recognized as one of the most important aerosols for climate forcing. In evaluating aerosol radiative effects, the mixing state of BC particles, namely, the degree to which BC particles are coated with other aerosol components, is a key parameter. Freshly emitted BC particles are generally bare (hydrophobic BC) and become internally mixed with other aerosols through condensation, coagulation, and photochemical oxidation processes in the atmosphere (referred to as "aging processes" hereafter). Coatings on BC particles with sufficient water-soluble compounds, such as ammonium sulfate $((NH_4)_2SO_4)$ and organic acids, change hydrophobic BC to

hydrophilic BC, which can serve as cloud condensation nuclei (CCN) at a given supersaturation. Therefore, the coatings on BC particles increase their wet scavenging efficiency and influence the atmospheric lifetime of BC Stier et al., (2006: Ref. 1) through their removal from the atmosphere by precipitation Oshima et al., (2012: Ref. 2). At the same time, coatings on BC particles with non-absorbing compounds enhance the BC absorption efficiency of solar radiation Bond et al., (2006: Ref. 3) This enhancement and the CCN activity of a BC-containing particle primarily depend on the diameters of the BC core and the particle shell, which consists of both the BC core and the coating materials. Consequently, to accurately estimate the aerosol optical properties and CCN activities of BC-containing particles,

one needs to know the entire BC mixing state, namely, the size distribution of BC-containing particles as a function of both the BC core diameter and the BC mass fraction. Although previous modeling studies have evaluated the radiative effects of aerosols including BC, some uncertainties remain in their results because the entire BC mixing state was not accurately treated in most of these studies.

In this study, a new mixing state resolved box model is developed to explicitly simulate the entire BC mixing state resulting from condensation/evaporation processes. This paper presents comparisons of the model simulation results with the aircraft observations and the influences of changes in the BC mixing state on aerosol optical properties and CCN activities for air parcels sampled by the aircraft.

2. Methods

A new box model, called Model of Aerosol Dynamics, Reaction, Ionization, and Dissolution (MADRID) [4] with resolution of the mixing state of BC (MADRID-BC), was developed as a stand-alone model that includes gas-phase chemistry. Oshima et al. (2009a, b: Ref. 5, 6) describe MADRID-BC in detail. MADRID-BC uses a 2-D aerosol representation, in which aerosol mass and number are given for individual particle diameters and BC mass fractions, so that the coexistence of BC particles with different shell diameters but with the same BC core diameter can be tracked for all ranges of BC core diameter (Figure 1). In this study, 40 size sections, ranging from 0.0215 μm to 10 μm, are employed, and BC mass fractions are divided into ten even sections between 0 and 100%. In addition to BC-containing particles, externally mixed "BC-free" particles are treated separately. Aerosol species treated in MADRID-BC include sulfate (SO_4^{2-}), ammonium (NH_4^+), nitrate (NO_3^-), sodium (Na^+), chloride (Cl^-), aerosol water, BC, and organic aerosol (OA). Note that the 2-D aerosol representation allows the coexistence of particles having different BC mass fractions with any given particle diameter. However, when aerosols are represented only by particle diameters, as used in most aerosol models (i.e., a one-dimensional (1-D) aerosol representation or a conventional sectional aerosol representation), the variability in aerosol mixing states cannot be represented.

MADRID-BC treats condensation/evaporation due to mass transfer between gas and particulate phases by a dynamic (kinetic) non-equilibrium approach developed by Meng et al. (1998: Ref. 7). BC aging processes due to coagulation and photochemical oxidation are not included in this study, although the contribution of coagulation may be important under certain circumstances. MADRID-BC treats heterogeneous reactions on the surface of particles and homogeneous nucleation processes [4], however, the nucleation process is not used in this study. The dilution of air, dry and wet deposition, and aqueous-phase chemistry in cloud particles are not included.
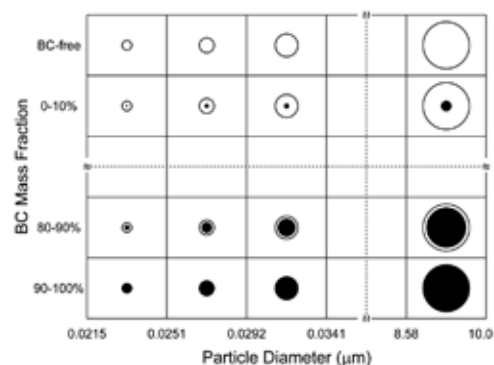
Figure 1 Schematic diagram of the two-dimensional (2-D) aerosol representation adopted in the MADRID-BC box model.

Aerosol optical properties (e.g., absorption and scattering coefficients of aerosol particles) are calculated based on the core-shell treatment according to the Mie code of Bohren and Huffman (1983: Ref. 8) for concentrically coated spheres. A complex refractive index of (1.85, –0.71i) at a wavelength of 550 nm [3] is used for the concentric core of pure BC. The CCN activities of BC-containing particles are estimated by calculating the critical supersaturation of particles with the Köhler equation. In this study, BC is treated as the insoluble concentric core of BC-containing particles, and other aerosol components are assumed to be soluble materials. When the critical supersaturation of BC-containing particles is lower than a given air supersaturation, these particles are defined as hydrophilic BC (i.e., CCN).

3. Results and discussion
3.1. Observed evolution of the BC mixing state

The Pacific Exploration of Asian Continental Emission phase C (PEACE-C) aircraft campaign was conducted over the western Pacific around Japan between 22 and 27 March 2004 [9]. Kinematic back trajectories of air parcels sampled from the aircraft were calculated using the method described by Tomikawa and Sato (2005: Ref. 10). Figure 2 shows two-day back trajectories for two air parcel groups, which were transported horizontally from over the Nagoya urban area, Japan, within the planetary boundary layer (PBL), during flight 5. Within air parcels sampled by the aircraft in the PBL, these two groups had the shortest (2 hours) and longest (13 hours) transport times over the ocean after leaving the coastline of Japan, and hereafter they are referred to as "fresh" and "aged" air, respectively. Both air parcels had likely been influenced by anthropogenic emission sources. During flight 5, the air parcels had very little chance to encounter clouds or precipitation.
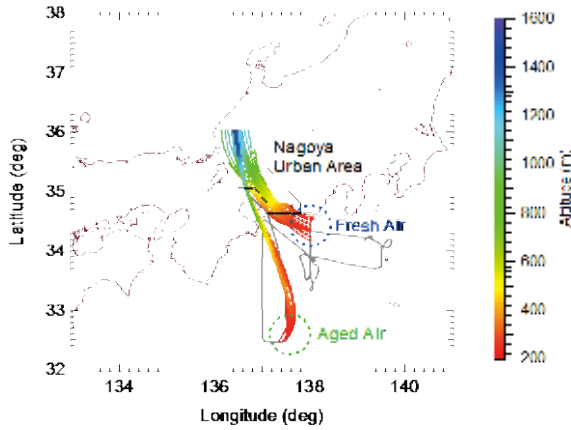
Figure 2 Flight tracks of the aircraft observations during PEACE-C flight 5 (gray lines) and two-day back trajectories of "fresh" and "aged" air parcels (colored lines).

Figure 3 Observed and model-predicted mass fractions of thickly-coated BC particles, $f_{thick}(D_{BC})$, defined by equation (1), as a function of the bulk $\Delta SO_4^{2-}/\Delta BC$ ratio. Results are shown for BC core diameters (D_{BC}) of 100–200 nm (model) and 155–185 nm (observation).

During the PEACE-C aircraft measurements, thinly- and thickly-coated BC particles were discriminated by using a single-particle soot photometer (SP2) [9]. These two types of aerosols generally correspond to BC particles with a shell/BC-core ratio smaller or greater than a particular threshold value. The mass fraction of thickly-coated BC particles, $f_{thick}(D_{BC})$, is defined for individual BC core diameters, D_{BC}, as follows,

$$f_{thick}(D_{BC}) = \frac{[BC_{thick}(D_{BC})]}{[BC_{thick}(D_{BC})] + [BC_{thin}(D_{BC})]} \quad (1)$$

where $[BC_{thick}(D_{BC})]$ and $[BC_{thin}(D_{BC})]$ are the total BC mass concentrations of thickly- and thinly-coated BC particles, respectively, for a given BC core diameter (D_{BC}).

Consistent with the shortest and longest transport times of the "fresh" and "aged" air parcels, the smallest and greatest $\Delta SO_4^{2-}/\Delta BC$ ratios were observed in "fresh" and "aged" air, respectively (Figure 3), where ΔSO_4^{2-} and ΔBC are the differences between observed and background concentrations of SO_4^{2-} and BC, respectively. In Figure 3, observed $f_{thick}(D_{BC})$ values are shown as a function of the $\Delta SO_4^{2-}/\Delta BC$ ratios for D_{BC} of 155–185 nm. Observed $f_{thick}(D_{BC})$ values increased continuously from 0.34 ("fresh" air) to 0.62 ("aged" air) as the $\Delta SO_4^{2-}/\Delta BC$ ratio increased from 1.3 to 3.5. This result shows that $f_{thick}(D_{BC})$ values increased as the photochemical production of SO_4^{2-} proceeded during transport. This increasing tendency can be viewed as a Lagrangian time evolution of the BC mixing state from "fresh" to "aged" air parcels during transport over the ocean.

3.2. Model-predicted evolution of BC mixing states

MADRID-BC was applied to the flight 5 case to validate the model simulations and examine changes in the entire BC mixing state. To simulate the entire BC mixing state in air sampled during flight 5, simulations for two consecutive regimes were performed. The simulation for the first regime
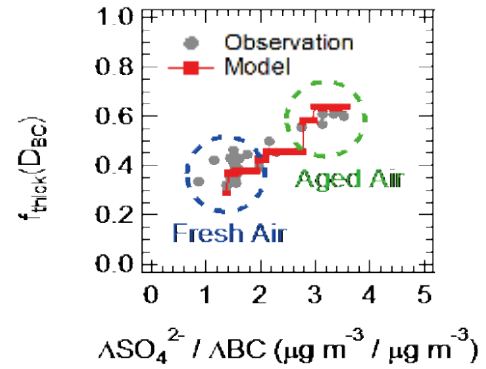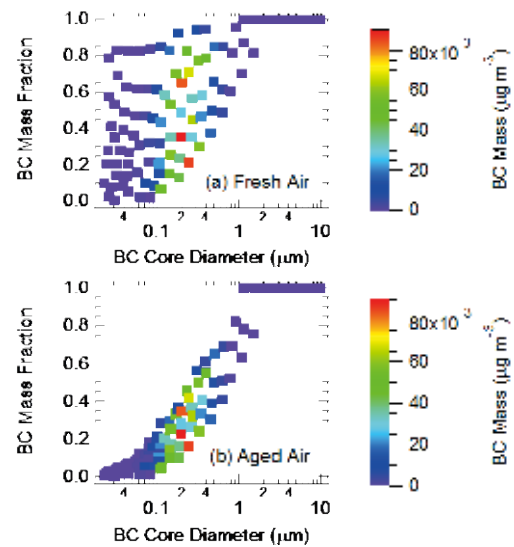
Figure 4 Entire BC mixing states predicted by the model for (a) "fresh" and (b) "aged" air parcels. The BC mass concentrations in individual grid cells are denoted by colored squares.

was for the source region, where emissions of BC particles were continuously introduced, and concurrent coatings due to condensation were calculated. The second regime simulation, which followed the first regime simulation, was for the outflow region over the ocean, where the coating process took place without emissions. These simulations were performed using observed bulk amounts of aerosols and gaseous concentrations as constraints so that the predicted bulk $\Delta SO_4^{2-}/\Delta BC$ ratio became equal to that observed in "fresh" and "aged" air, respectively.

As shown in Figure 3, MADRID-BC reproduced well the observed increase in $f_{thick}(D_{BC})$ values with the increase in the $\Delta SO_4^{2-}/\Delta BC$ ratio from "fresh" to "aged" air for the observed BC core diameter ranges. The agreement in $f_{thick}(D_{BC})$ values of this particular case suggests the validity of the time evolution of the model-predicted entire BC mixing state. The validity found in this study also suggests that

general features of the evolution of BC mixing states can be interpreted at least by the condensational growth process in this particular case.

In the predicted entire BC mixing states for "fresh" and "aged" air (Figures 4a and 4b, respectively), BC-containing particles with different BC mass fractions (coating thicknesses) coexist for individual BC core diameters. The mass of BC particles is concentrated at a BC core diameter of around 200 nm, reflecting the input BC core size distribution. Comparison of the entire BC mixing state between "fresh" and "aged" air shows two distinguishing features. First, compared with "fresh" air, BC mass fractions in "aged" air are systematically smaller for particles with BC core diameters smaller than 1 μm, and BC mass fractions of smaller BC particles show larger decreases. Second, the spread of the BC mass fraction at a given individual BC core diameter is systematically smaller in "aged" air than in "fresh" air. These two features are consistent with both condensation theory, which predicts that the rate of change in particle diameter is greater for a smaller particle, and also with the absence of BC emissions in the outflow region over the ocean, in contrast to continuous emissions of uncoated BC over the source region.

3.3. Aerosol optical properties and CCN activities

Aerosol optical properties were estimated at a wavelength of 550 nm using MADRID-BC based on the validated BC mixing states for "fresh" and "aged" air parcels (Table 1). In this particular case, the BC coatings enhance the overall absorption of particles by 38% and 59% in "fresh" and "aged" air, respectively. The overall single scattering albedo (SSA) of particles increases from 0.81 in "fresh" air to 0.85 in "aged" air. CCN activities were also estimated for a supersaturation of 0.05% for "fresh" and "aged" air parcels (Table 1). The overall hydrophilic BC mass fraction increases from 0.55 in "fresh" air to 0.83 in "aged" air, although these values are quite sensitive to the given supersaturation. This result suggests the importance of the uplift of BC particles near source regions for their efficient long-range transport through the free troposphere, because precipitation generally takes place in association with vertical transport of air.

Another simulation using a conventional sectional (1-D) aerosol representation was conducted to evaluate possible errors in aerosol optical properties and CCN activities calculated using the 1-D aerosol representation instead of the BC-mixing-state-resolved (2-D) aerosol representation (Table 1). In comparison with the 2-D aerosol representation results, the 1-D case simulation gives considerably larger overall absorption coefficients (by 35–44%), a much smaller overall SSA (by 7.2–13%), and a larger overall fraction of hydrophilic BC mass (by 7.9–34%) for particles in air. The absence of efficiently scattering BC-free particles in the conventional sectional (1-D) aerosol representation, which causes not only smaller scattering effects but also greater

coating amounts on BC-containing particles, can explain these differences. These results demonstrate the importance of a BC-mixing-state-resolved aerosol representation in aerosol modeling to accurately predict the optical properties and CCN activities of BC particles.

Table 1 Aerosol optical properties and CCN activities calculated by MA-DRID-BC using a 2-D aerosol representation and a conventional sectional (1-D) aerosol representation (in parentheses)

Parameter	Fresh air	Aged air
Extinction coefficient	75.1 (69.7)	107 (103)
Scattering coefficient	60.9 (49.3)	90.9 (80.8)
Absorption coefficient	14.2 (20.4)	16.4 (22.1)
Absorption amplification	1.38 (1.77)	1.59 (1.92)
Single scattering albedo	0.811 (0.708)	0.847 (0.786)
Fraction of hydrophilic BC mass	0.552 (0.738)	0.831 (0.897)

1 Stier, P., J. H. Seinfeld, S. Kinne, J. Feichter and O. Boucher 2006: Impact of nonabsorbing anthropogenic aerosols on clear-sky atmospheric absorption, *J. Geophys. Res.,* **111**, D18201, doi: 10.1029/2006JD007147.

2 Oshima, N., Y. Kondo, N. Moteki, N. Takegawa, M. Koike, K. Kita, H. Matsui, M. Kajino, H. Nakamura, J. S. Jung and Y. J. Kim, 2012: Wet removal of black carbon in Asian outflow: Aerosol Radiative Forcing in East Asia (A-FORCE) aircraft campaign, *J. Geophys. Res.,* **117**, D03204, doi: 10.1029/2011JD016552.

3 Bond, T. C., G. Habib and R. W. Bergstrom, 2006: Limitations in the enhancement of visible light absorption due to mixing state, *J. Geophys. Res.,* **111**, D20211, doi: 10.1029/2006JD007315.

4 Zhang, Y., B. Pun, K. Vijayaraghavan, S. Wu, C. Seigneur, S. N. Pandis, M. Z. Jacobson, A. Nenes, and J. H. Seinfeld 2004: Development and application of the Model of Aerosol Dynamics, Reaction, Ionization, and Dissolution (MADRID), *J. Geophys. Res.,* **109**, D01202, doi: 10.1029/2003JD003501.

5 Oshima, N., M. Koike, Y. Zhang, Y. Kondo, N Moteki, N. Takegawa and Y. Miyazaki, 2009a: Aging of black carbon in outflow from anthropogenic sources using a mixing state resolved model: Model development and evaluation, *J. Geophys. Res.,* **114**, D06210, doi:10.1029/2008JD010680.

6 Oshima, N., M. Koike, Y. Zhang and Y. Kondo, 2009b: Aging of black carbon in outflow from anthropogenic sources using a mixing state resolved model: 2. Aerosol optical properties and cloud condensation nuclei activities, *J. Geophys. Res.,* **114**, D18202, doi:10.1029/2008JD011681.

7 Meng, Z., D. Dabdub and J. H. Seinfeld, 1998: Size-resolved and chemically resolved model of atmospheric aerosol dynamics, *J. Geophys. Res.,* **103**, 3,419–3,435.

8 Bohren, C. F. and D. R. Huffman, 1983: *Absorption and Scattering of Light by Small Particles*, John Wiley, Hoboken, N. J.

9 Moteki, N., Y. Kondo, Y. Miyazaki, N. Takegawa, Y. Komazaki, G. Kurata, T. Shirai, D. R. Blake, T. Miyakawa and M. Koike, 2007: Evolution of mixing state of black carbon particles: Aircraft measurements over the western Pacific in March 2004, *Geophys. Res. Lett.,* **34**, L11803, doi: 10.1029/2006GL028943.

10 Tomikawa, Y. and K. Sato, 2005: Design of the NIPR trajectory model, *Polar Meteorol. Glaciol.,* **19**, 120-137.

Formation and variations of aerosols around Beijing using the WRF-chem model

Hitoshi Matsui[1,*], Makoto Koike[1], Yutaka Kondo[1] and Nobuyuki Takegawa[1]

[1]University of Tokyo, Hongo 7-3-1, Bunkyo-ku, Tokyo 113-0033, Japan

*Corresponding author. Tel.: +81 3 5841 4550; Fax: +81 3 5841 8318, Email address: matsui@eps.s.u-tokyo.ac.jp (H. Matsui)

Model calculations were conducted with the Weather Research and Forecasting model coupled with a chemistry scheme (WRF-chem) for the region around Beijing, China, in summer 2006, when the CAREBeijing-2006 intensive campaign was conducted. In this paper, we interpret aerosol optical properties in terms of aerosol mass concentrations and their chemical compositions by linking model calculations with measurements.

1. Introduction

The mega-cities of East Asia are large emission sources that have considerable impacts on regional climate and air quality. We performed three-dimensional aerosol model simulations for the region around Beijing with the Weather Research and Forecasting model coupled with a chemistry scheme (WRF-chem). The purposes of this study were (1) to validate the model-simulated spatial and temporal variations of aerosol mass concentrations and optical properties and (2) to systematically understand the spatial and temporal variations of aerosol mass concentrations and their optical parameters around Beijing. This study is one of the first applications of the WRF-chem model to the simulation of aerosol optical properties associated with mega-city emissions in East Asia.

2. Methods

2.1. Three-dimensional model (WRF-chem)

WRF-chem version 2.2 was used as a regional three-dimensional model [1, 2]. The details of the calculation settings and parameterization schemes used are described elsewhere [3, 4]. Model calculations were conducted for two domains with horizontal resolutions of 27 and 9 km. The simulation period was from 10 August to 11 September 2006. For the aerosol calculations, the Model for Simulating Aerosol Interactions and Chemistry (MOSAIC) was used, and a sectional representation of the aerosol size distribution was adopted to simulate both particle number and mass in each aerosol size bin [2, 5]. An eight-bin representation was adopted. Aerosol species included were sulfate, nitrate, ammonium, elemental carbon (EC), primary

organic aerosols, nonreactive dust, and aerosol water. Anthropogenic emission inventories for 2004 were used [3, 6]. The Global Emissions Inventories Activity [7] was used for biogenic emission inventories.

Aerosol optical parameters were calculated offline using the WRF-chem-simulated aerosol mass concentration and size distributions, rather than using those calculated online, within WRF-chem. The offline optical calculation approach adopted an algorithm based on Mie theory [8] to estimate differences in aerosol optical properties calculated using three different aerosol mixing state treatments, namely, well-mixed internally (WMI), core-shell internally mixed (CSI), and externally mixed (EM) [4]. Here, we mainly use the aerosol optical properties calculated using the WMI treatment (at 550 nm) in the comparison with the measurement data, because this treatment was also used in the online WRF-chem calculations.

2.2. Measurements

Model calculations of aerosol optical properties were compared with various in situ measurements made during the CAREBeijing-2006 campaign, which was conducted between 10 August and 11 September 2006. Intensive aerosol measurements were carried out at Yufa, a site about 50 km south of Beijing. Details of the observation sites and CAREBeijing-2006 measurements are reported in other papers [9, 10]. In this study, we used mass concentrations of inorganics (obtained with an Aerodyne Aerosol Mass Spectrometer), EC/organic carbon (OC) (Sunset Laboratory semi-continuous EC/OC analyzer), and $PM_{2.5}$ (tapered element oscillating microbalance), aerosol size distributions

(twin differential mobility particle sizer and aerodynamic particle sizer), the absorption coefficient (b_{abs}) at 532 nm (photoacoustic spectrometer), and the scattering coefficient (b_{scat}) at 550 nm (nephelometer).

3. Results: mass and optical properties
3.1. Variations in aerosol mass concentrations

Model calculations generally captured the temporal variations of primary (such as EC) and secondary (such as sulfate) aerosols observed at Yufa (Figure 1). Model calculations showed distinct differences in spatial distribution between primary and secondary aerosols in association with synoptic-scale meteorology. Under an anticyclonic pressure system, secondary aerosols increased in the air around Beijing within an area of about 1000×1000 km^2. This polluted air mass had been transported northward from the area of high anthropogenic emissions and continuous photochemical production in the region south of Beijing. Then, the subsequent passage of a cold front brought clean air from the north, and the polluted air around Beijing was swept southward. This cycle was repeated about once a week and was found to be responsible for observed enhancements and reductions of aerosols at the intensive measurement sites. In contrast to the secondary aerosols, the spatial distributions of primary aerosols (EC) reflected those of emissions, resulting in only slight variability despite changes in the synoptic-scale meteorology. In accordance with these results, source apportionment simulations revealed that primary aerosols in Beijing were controlled by emissions emitted within 100 km of Beijing and within the preceding 24 hours, whereas emissions emitted as far as 500 km of Beijing and within the preceding 3 days were found to affect secondary aerosols.
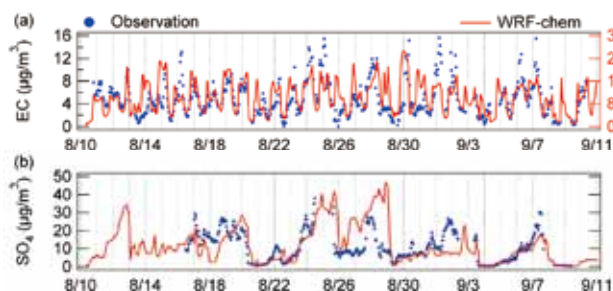
Figure 1 Time series of (a) EC and (b) sulfate at the Yufa site.

3.2. Variations in aerosol optical properties

Model calculations generally reproduced well the temporal variability of the local aerosol optical properties at Yufa (Figure 2). Because of the reasonable agreement with measurements, spatial and temporal variations of aerosol optical properties around Beijing were interpreted from the model results from the viewpoint of regional-scale aerosol mass distributions of individual chemical components. The spatial and temporal variations of b_{abs}, b_{scat}, and the extinc-

tion coefficient (b_{ext}) and the single scattering albedo (SSA) corresponded well to those of the mass concentrations of EC, sulfate, and PM$_{2.5}$, and the mass fractions of secondary aerosols, respectively. Therefore, aerosol optical parameters can be interpreted by considering in combination the spatial variations of EC, which are controlled by local-scale emissions (within 100 km of Beijing during the preceding 24 h), and those of sulfate, which are controlled by regional-scale emissions (within 500 km of Beijing during the preceding 3 days), as well as by synoptic meteorological conditions. These results explain why b_{scat} and b_{ext} exhibited multi-day variations, whereas b_{abs} primarily exhibited diurnal variations at Yufa.

On the other hand, the model calculations underestimated the absolute values of b_{ext}, b_{scat}, and SSA by 40%, 50%, and 20%, respectively, and overestimated the absolute value of b_{abs} by 60%. The underestimation and overestimation exceed the uncertainties in the measurements. Possible causes of the discrepancies between measurements and model calculations are discussed in section 3.3

.

3.3. Offline sensitivity calculations

Here we discuss possible factors accounting for the overestimation and underestimation by the aerosol optical parameter calculations, including uncertainties in the aerosol physical parameters (aerosol density and refractive index), size distribution, and mixing state (adopted for aerosol optical calculations). We first examine b_{ext} (sections 3.3.1 and 3.3.2) because it is rather insensitive to the aerosol mixing state, and we examine the other optical parameters (b_{abs}, b_{scat}, and SSA) in section 3.3.3.
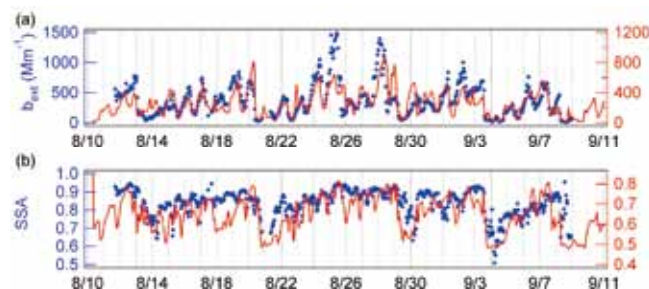
Figure 2 Time series of (a) b_{ext} and (b) SSA at the Yufa site.

3.3.1. Total mass and b_{ext}

We examine closure among the measurements themselves in terms of aerosol mass, size distribution, and optical properties to separate the uncertainties in the model calculations from those in the measurements. First, we examine the closure between aerosol mass concentrations and size distributions. When we estimated PM$_{2.5}$ mass concentrations from the size distribution measurements using an aerosol density of 1.6 g cm^{-3}, as assumed in the aerodynamic particle sizer measurements [11], their absolute values and temporal variation agreed with those of measured

$PM_{2.5}$ within the uncertainty of the measurements.

Second, we examine the closure between b_{ext} and size distributions. We estimated b_{ext} values of PM_{10} from the measured size distribution and chemical composition by the WMI treatment. When we compared these with the measurements obtained by the photoacoustic spectrometer and nephelometer, they agreed within 3%. We also found a quite good agreement of their temporal variations (correlation coefficient = 0.99 for hourly data).

We found reasonably good measurement closure, within the uncertainties in observed aerosol mass, size distribution, and b_{ext} values. These results suggest that the disagreement in b_{ext} values between measurements and model calculations is not due to the Mie theory algorithm itself but instead is due mainly to the uncertainties/errors in the parameters used for the Mie calculations, such as the refractive index and the size distributions of aerosols in the model calculations.

3.3.2. Aerosol density, refractive index, and size distribution: b_{ext}

The average aerosol density in the WRF-chem calculations of approximately 2.0 g cm^{-3} was greater than the density of 1.6 g cm^{-3} assumed in the measurements [11]. This discrepancy is partly because the density of unidentified species is unknown and a high aerosol density (2.6 g cm^{-3}) is assumed for dust species in the model calculations. Some organic aerosols in the real atmosphere with densities as low as 1 g cm^{-3} may also contribute to this discrepancy, because they are not included in our WRF-chem calculations. In addition, non-spherical aerosol particles in the real atmosphere (under dry conditions) may in part account for this discrepancy because spherical particles are assumed in the model calculations. In this study, the discrepancy in "aerosol density" between measurements and model calculations includes all of the above potential effects related to mass-to-volume conversion.

The period average of the volume-averaged aerosol refractive index in the WRF-chem calculations is 1.545 + 0.091i, whereas an estimate obtained by using the observed PM_1 chemical composition is 1.545 + 0.103i. Consequently, errors due to the refractive index are expected to be small in this study.

To obtain a quantitative understanding of the discrepancies in b_{ext} between model calculations and measurements, we conducted simple sensitivity studies in which model-calculated aerosol density, refractive index, and the shape of the size distribution were individually replaced with values estimated from the measurements. In these sensitivity calculations, total aerosol mass concentrations at each time point were constrained by the results of the WRF-chem calculations. In addition, we assumed that aerosol density and refractive index did not influence each other (e.g., we used measurement-derived density with the model-calculated refractive index). Note that the replacement of the refractive index, aerosol density, and the shape of size

distribution is equivalent to making changes in chemical composition, volume, and the size distribution with constant volume, respectively.

The use of measurement-derived values for both density and the refractive index causes a 37% increase in b_{ext} (orange square in Figure 3a), leading to much better agreement with the measurements (blue circle in Figure 3a). Most of the increase was due to the aerosol density change (28% increase in b_{ext}) because a lower density (1.6 g cm^{-3} instead of 2.0 g cm^{-3}) results in a larger total aerosol volume and mass extinction efficiency and therefore a larger b_{ext} value.

Similarly, we conducted sensitivity calculations to estimate errors in b_{ext} caused by errors in the shape of the aerosol size distributions calculated by WRF-chem. In this sensitivity calculation we used the shape of the observed aerosol size distributions without changing the model-calculated aerosol total mass, density, or volume-averaged refractive index. As a result, the period-averaged b_{ext} value increased by 9.1% (green square in Figure 3a).

Finally, we conducted sensitivity calculations in which all three aerosol parameters (aerosol density, refractive index, and the shape of the size distribution) were replaced with measurement-derived values, while using model-calculated mass concentrations. As a result, the calculated b_{ext} value (black square in Figure 3a) agrees with observed b_{ext} within 0.5%.

These sensitivity calculations demonstrate that the discrepancies in b_{ext} between the calculations and measurements are due mostly to the treatment of aerosol density (disagreement between the calculated mass-to-volume conversion and the measurements) in the model calculations.
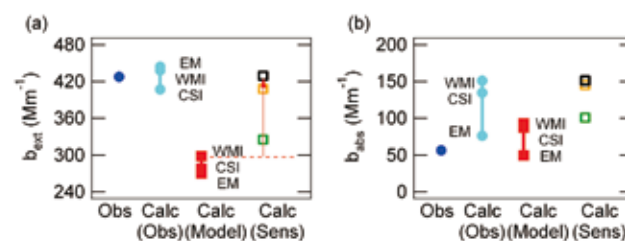
Figure 3 Period-averaged (a) b_{ext} and (b) b_{abs} at Yufa. The results of the optical sensitivity calculations are also shown.

The contributions of the refractive index and the shape of the size distribution to b_{ext} discrepancies were estimated to be small. Good agreement with measurements is achieved when these aerosol properties are accurately predicted or assumed; however, a notable bias can result when these properties are inadequately treated, even if total aerosol mass concentrations are reproduced well in the model calculations.

3.3.3. Aerosol mixing states: b_{abs}, b_{scat}, and SSA

Optical parameters were also estimated from the ob-

served size distribution and chemical composition for the CSI and EM aerosol mixing state treatments. Although b_{ext} was insensitive to the aerosol mixing state treatment, b_{abs} and SSA were sensitive to the treatment and agreed better with direct measurements when the EM treatment was adopted (Figure 3b). These results are consistent with the observed features of the aerosol mixing states during the CAREBeijing-2006 campaign [11].

When b_{abs} and SSA were calculated using the results of the WRF-chem calculations, similar tendencies were found: namely, b_{abs} values were largest (lowest) and SSA values were lowest (largest) when the WMI (EM) treatment was adopted. Because the aerosol mixing state is essential information for reproducing SSA in model calculations, it is quite important to improve regional aerosol models to represent multiple mixing states and their aging processes.

4. Summary

Regional aerosol model calculations were made using WRF-chem to study spatial and temporal variations of aerosol mass concentrations of individual chemical components and their optical properties around Beijing, China. Model calculations reproduced the temporal variations of aerosol mass concentrations and optical properties observed during the CAREBeijing-2006 campaign.

The spatial and temporal variations of the absorption, scattering, and extinction coefficients and SSA corresponded well with those of the mass concentrations of EC, sulfate, and $PM_{2.5}$ and the mass fractions of secondary aerosols, respectively. Therefore, aerosol optical parameters can be interpreted by considering the combination of spatial variations of primary aerosols (EC), which are controlled by local-scale emissions, and those of secondary aerosols (sulfate), which are controlled by regional-scale emissions, along with synoptic meteorological conditions. These results explain why the scattering and extinction coefficients exhibited multi-day variations, while the absorption coefficient primarily exhibited diurnal variations, at Yufa.

Model calculations, however, underestimated or overestimated the absolute levels of aerosol optical properties around Beijing by up to 60%. Offline sensitivity calculations showed that the treatment of aerosol mixing states and aerosol "density" (parameters related to mass-to-volume conversion) in the model calculations mainly contributed to these over- and underestimations. Good agreement with measurements is achieved when these aerosol parameters are accurately predicted or assumed; however, a notable bias can result when these properties are inadequately treated, even if total aerosol mass concentrations are reproduced well in the model calculations.

1 Grell, G. A., S. E. Peckham, P. Schmitz, et al. 2005: Fully coupled "online" chemistry within the WRF model, *Atmos. Environ*, **39**, 6,957 – 6,975.

2 Fast, J. D., W. I. Gustafson, R. C. Easter, et al. 2006: Evolution of ozone, particulates, and aerosol direct radiative forcing in the vicinity of Houston using a fully coupled meteorology-chemistry-aerosol model, *J. Geophys. Res.*, **111**: D21305, doi: 10.1029/2005JD006721.

3 Matsui, H., M. Koike, Y. Kondo, et al. 2009: Spatial and temporal variations of aerosols around Beijing in summer 2006: Model evaluation and source apportionment, *J. Geophys. Res.,* **114**: D00G13, doi: 10.1029/2008JD010906.

4 Matsui, H., M. Koike, Y. Kondo, et al. 2010: Spatial and temporal variations of aerosols around Beijing in summer 2006: 2. Local and column aerosol optical properties, *J. Geophys. Res.,* **115**: D22207, doi: 10.1029/2010JD013895.

5 Zaveri, R. A., R. C. Easter, J. D. Fast, et al. 2008: Model for Simulating Aerosol Interactions and Chemistry (MOSAIC), *J. Geophys. Res.*, **113**: D13204, doi: 10.1029/2007JD008782.

6 Zhang, Q., D. G. Streets, G. R. Carmichael, et al. 2009: Asian emissions in 2006 for the NASA INTEX-B mission, *Atmos. Chem. Phys.*, **9**, 5,131 – 5,153.

7 Guenther, A., C. N. Hewitt, D. Erickson, et al. 1995: A global model of natural volatile organic compound emissions, *J. Geophys. Res.*, **100**, 8,873 – 8,892.

8 Bohren, C. F., and D. R. Huffman, 1998:Absorption and Scattering of Light by Small Particles, John Wiley, Hoboken, N. J.

9 Takegawa, N., T. Miyakawa, M. Kuwata, et al. 2009: Variability of submicron aerosol observed at a rural site in Beijing in the summer of 2006, *J. Geophys. Res.*, **114**: D00G05, doi: 10.1029/2008JD010857.

10 Garland, R. M., O. Schmid, A. Nowak, et al. 2009: Aerosol optical properties observed during Campaign of Air Quality Research in Beijing 2006 (CAREBeijing-2006): Characteristic differences between the inflow and outflow of Beijing city air, *J. Geophys. Res.*, **114**: D00G04, doi: 10.1029/2008JD010780.

11 Cheng, Y. F., M. Berghof, R. M. Garland, et al. 2009: Influence of soot mixing state on aerosol light absorption and single scattering albedo during air mass aging at a polluted regional site in northeastern China, *J. Geophys. Res.*, **114**: D00G10, doi: 10.1029/2008JD010883.

Shape modeling of dust and soot particles for remote sensing applications by considering the geometrical features of sampled aerosols

Hiroshi Ishimoto[1*], Yuji Zaizen[2], Kazuhiko Masuda[1], Yuzo Mano[1] and Akihiro Uchiyama[3]

[1]Meteorological Satellite and Observation System Research Department, Meteorological Research Institute, 1-1 Nagamine, Tsukuba, Ibaraki 305-0052, Japan
[2]Atmospheric Environment and Applied Meteorology Research Department, Meteorological Research Institute, 1-1 Nagamine, Tsukuba, Ibaraki 305-0052, Japan
[3]Climate Research Department, Meteorological Research Institute, 1-1 Nagamine, Tsukuba, Ibaraki 305-0052, Japan

*Corresponding author. Tel.: +81 29 853 8676; Fax: +81 29 856 0644, Email address: hishimot@mri-jma.go.jp
  (H. Ishimoto)

   We present shape models for dust and soot particles that were developed by taking into account the geometrical features of sampled aerosols and using an assumed cell-type structure. We examined the spatial Poisson-Voronoi tessellation by considering the assumed basic structure of the material, and determined the particle shapes by extracting cells from the tessellation. Using these procedures, hundreds of "Voronoi aggregates" were prepared for use in a dust particle model. To determine the final model, we used two-dimensional images of dust particles collected at Fukuoka, Japan, on 16 March 2009, during a time when dust particles transported from China were widely observed in this part of western Japan. For the shape analysis, we used silicate-dominated particles, which were identified by transmission electron microscopy spectral analysis. For the modeling of soot particles, selected fractal structures with arbitrary fractal dimensions were examined and compared to the sampled images of complex-shaped aerosols, under the assumption that the aerosol particles with highly complex shapes were soot particles. A database of the optical properties of these aerosol models was compiled from calculations by the finite-difference time-domain method, the geometric optics integral equation method, and a conventional geometric optics method. The database will be made available for use in analyses of aerosol remote sensing data.

Keywords: Mineral dust; Soot; Irregular shape; Optical modeling

1. Introduction

   Together with particle size and chemical composition, the shape characteristics of aerosol particles must be considered in their optical modeling. Because dust and soot particles generally have irregular and complex shapes, some models assuming simple shapes (e.g., spheres and spheroids) may produce large errors when estimating the radiative properties of particles in the visible and near-infrared wavelengths. There is also an increasing demand for models using realistic aerosol shapes for various applications of multi-channel and polarization observations by satellite and ground-based active or passive sensors.

   With advances in computer performance, it is possible to create a database of the optical properties of modeled particles over a wide size range that takes into account their realistic shapes and structures. For nonspherical and inhomogeneous particles with small size parameters $x = \pi d / \lambda$, where d is the size of the particle and λ is the wavelength, discrete-dipole approximation and finite-difference time-domain (FDTD) methods are widely used for the accurate determination of their light-scattering properties. These numerical methods can be used for most of the typical size range of soot particles at visible and near-infrared wavelengths.

   For relatively large aerosol particles, such as mineral dust, improved geometrical optics approximations (GOM2 or geometric optics integral equation: GOIE), which use the integral equation of electromagnetic wave theory, produce reasonably accurate results (e.g., [1, 2]). Therefore, formulating realistic and sophisticated aerosol shape models for use with these numerical methods is vital for improving remote sensing analysis and radiative models of the atmosphere. To create realistic shape models, geometrical information collected from microscopic images of sampled aerosols is important.

   In this paper, we propose an approach for modeling the three-dimensional shape of mineral dust and soot particles

from geometrical information provided by aerosol images.

2. Methods

Shape models of mineral dust and soot particles were created by the following procedure.

(i) The basic structure of the shape model was obtained by applying certain microphysical assumptions.

(ii) By a Monte Carlo approach, a number of particle models were created by changing various parameters to modify the shape characteristics of the structure assumed in (i).

(iii) A final shape model was determined by statistical comparison of two-dimensional geometrical features between randomly oriented model particles and sampled aerosols.

In this method, the basic structure assumed in (i) is crucial for producing a reasonable shape model. The final shape model determined was not a copy of a specific aerosol particle seen in the microscopic images, but a virtual particle with geometrical features similar to those of an ensemble average of the sampled aerosols. The intention was to simulate the average optical properties of the sampled aerosols by using a small number of shape models in order to reduce the computational cost of light-scattering calculations.

2.1. Mineral dust model

We used a spatial Poisson-Voronoi tessellation to simulate the basic structure of mineral dust particles [3]. A Poisson-Voronoi structure has been used as a simple crystal growth model in structural analysis studies [4], where the structure is defined by nucleation points within a numerical field. The structure consists of Voronoi cells with each cell sharing a facet with a neighboring cell, and aggregates of Voronoi cells (hereafter, Voronoi aggregate: VA) are determined by extracting the cells enclosed within an assumed spheroid. Therefore, the shape of the VA depends on the number of initial nucleation points and their locations in the numerical field, and on the shape of the assumed outer spheroid. In this study, we randomly selected 100 nucleation points in the numerical field and then examined different spheroid shapes, creating hundreds of aggregates for each combination of tessellation and outer spheroid. Examples of numerically created VAs are shown in Figure 1.
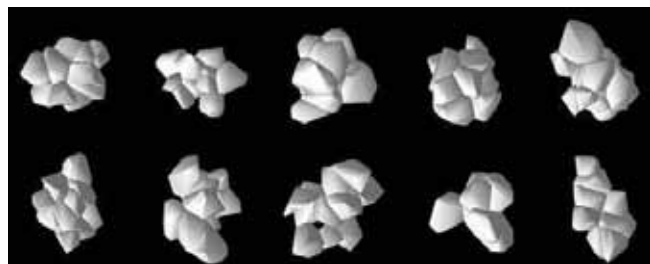
Figure 1 Examples of numerically created Voronoi aggregates

To determine the mineral dust shape model from the large number of created VA particles, geometrical information obtained from microscopic images of sampled aerosols was considered. For the shape analysis, images of particles larger than 0.1 μm were used. Furthermore, silicate-dominated particles (Si weight ratio more than 65%) were chosen following chemical analysis with an energy-dispersive X-ray (EDX) analyzer. We also removed particles that included materials soluble in water or other liquids detected by electron beam irradiation. These elemental analyses were performed on 91 particles on the sample plate, leaving 18 particles for image analysis (see Figure 2).
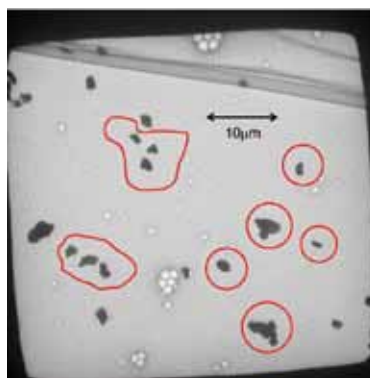
Figure 2 Microscopic image of aerosols sampled at Fukuoka, Japan, on 16 March 2009. Mineral dust particles identified by EDX analysis are encircled by red lines.

We calculated two non-dimensional shape parameters (α, β) for the 18 dust particle images and numerically created VAs:

$$\alpha \equiv \frac{4A}{\pi D^2}, \ \beta \equiv \frac{4\pi A}{L^2} \qquad (1)$$

where A is the area, D is the maximum dimension, and L is the perimeter of the projected particle image. Figure 3 shows scatter plots of (α, β) for the 18 mineral dust particle samples (Figure 3a) and for 100 VAs created by using a prolate spheroid with an axis ratio of 1:2 for the outer shape (Figure 3b).
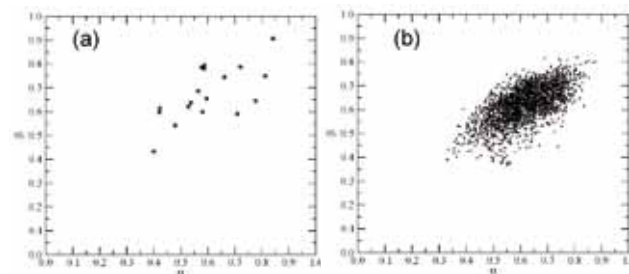
Figure 3 Scatter plots of the geometrical parameters (α, β) of 18 aerosol particles (a) and 100 selected Voronoi aggregates (VAs) (b) The calculated values for 46 orientations of each VA are plotted.

By using a least-squares analysis for correlation of the (α, β) distribution, we determined the final shape model for mineral dust particles. The resultant shape model consisted of four Voronoi cells and was relatively simple compared with other possible shape models (Figure 1). Because of the small number of mineral dust samples, we neglected the particle size dependence of (α, β) and proposed only one shape model.
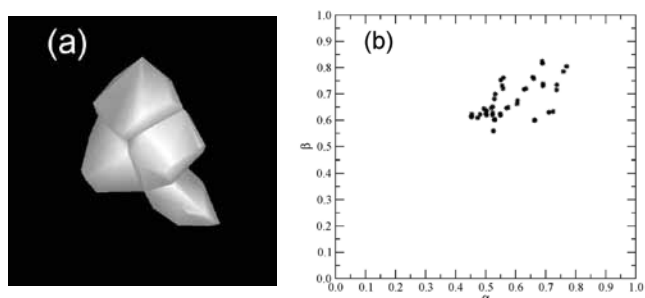
Figure 4 Shape model for mineral dust particles (a) and the (α, β) distribution of its 46 orientations (b).

2.2. Soot model

There is a large body of previous work on determining soot particle shape. A typical assumption is that soot particles consist of primary particles (monomers) and have a fractal structure with a specific fractal dimension (e.g., Ref. [5]). We also assumed a fractal structure for soot particles. Moreover, we considered aerosol particles with a highly complex structure on the microscopic images to be soot and used them as the reference soot particles, because it was difficult to identify soot particles directly by elemental analysis. From microscopic images of aerosol samples obtained at Tsukuba, Japan, we selected 52 complex-shaped aerosols with the geometrical parameter $\beta \leq 0.3$ and assumed that they were soot particles (Figure 5).

We created many fractal structures with a specific fractal dimension d_f between 1.5 and 2.4 at intervals of 0.1, by using the numerical procedure described in [6]. Then we created spatial Poisson-Voronoi tessellations with an average cell size of ~30 nm. To restrict the size variation for each Voronoi cell, a Matérn hard-core point field (e.g., Ref. [4]) was applied to determine the distribution of the initial nucleation points for generating tessellations. After applying the prepared fractal structure to the Voronoi tessellation, Voronoi cells that overlapped the fractal shape were extracted [7]. Examples of aggregates of Voronoi cells are shown in Figure 6.

Figure 5 Reference particles for soot modeling selected from microscopic images. The largest particle has $D = \sim 3$ μm.
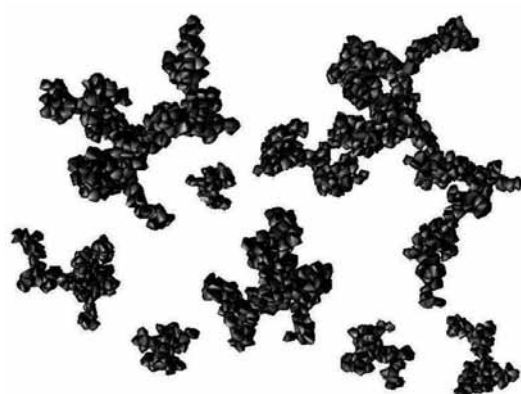
Figure 6 Voronoi aggregates created by using fractal structures (fractal dimension $d_f = 1.7$ in box-count method).

Figure 7 shows the geometrical parameters α and β with respect to the maximum dimension D for the soot particles and for the orientation-averaged fractal aggregates, where 10 size categories and 10 modeled particles of each size were used for the fractal aggregate. For particles with $D \geq 1$ μm, the aggregates with fractal dimensions between 1.5 and 1.8 agreed well with the selected soot samples, for both parameters α and β. However, a bias was confirmed in values of β for particles with $D \leq 0.5$ μm. Because we considered the average cell size of the aggregate to be 30 nm, the small modeled aggregates became more compact than the sampled soot particles. This result indicates that it is difficult to simulate the size dependence of the shape properties of whole soot particles, such as those shown in Figure 5, by using only one fractal dimension and one average monomer size. To improve the $\beta - D$ relationship for the modeled particles, we further considered the particle size dependence of the monomer (size of the Voronoi cell). The final soot model was selected from 10 sets of modified fractal aggregates with a fractal dimension $d_f = 1.7$ (Figure 8).
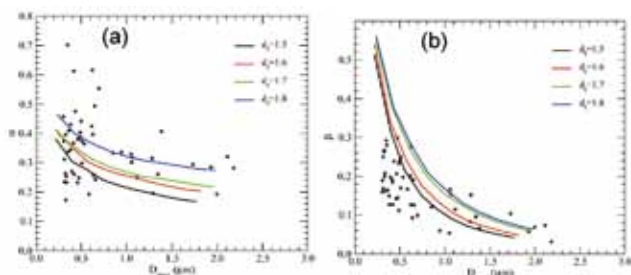
Figure 7 Size dependence of the geometrical parameters α (a) and β (b) for the assumed soot particles (*) and the simulated fractal-Voronoi aggregates with fractal dimensions $d_f = 1.5 - 1.8$ (lines).
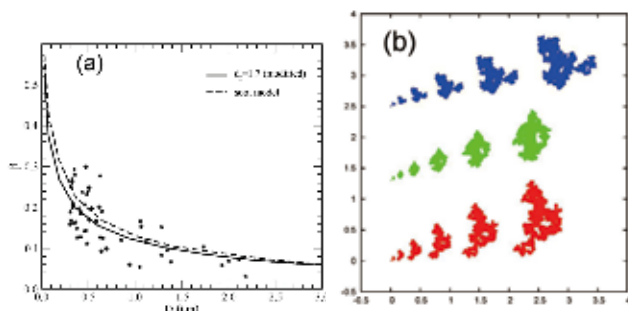
Figure 8 (a): The same as Figure 7b but for particles with modified $d_f = 1.7$ (solid line) and for the soot shape model determined by light scattering calculations (dashed line). (b): The shapes of six soot models of different sizes. Different colors indicate views from different angles.

3. Database of optical properties

Optical properties of the mineral dust and soot models were calculated by using FDTD, GOIE, and conventional geometrical optics methods for various size parameters and refractive indices. A database of these optical properties is scheduled to be used for data analysis by the Second-generation Global Imager onboard the Global Change Observation Mission Climate (GCOM-C1) satellite. Furthermore, we inserted our mineral dust model, called MRIDUST, into the RSTAR atmospheric radiative transfer model developed by the Atmosphere and Ocean Research
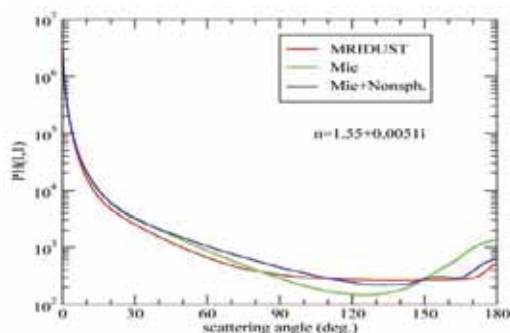
Figure 9 Size averaged phase function of the mineral dust model MRIDUST (red), based on the size distribution of the "yellow sand" model in the RSTAR code and refractive index $n = 1.55 + 5.102 \times 10^{-3} i$ at wavelength $\lambda = 0.5\mu m$. Results of the Mie calculation (green) and the Mie calculation modified by an empirical formula for nonsphericity (blue) are shown for comparison.

Institute, Tokyo University [8], as an optional calculation scheme for "Yellow sand" (i.e., mineral dust) (currently only available to model developers).

4. Discussion

Mineral dust and soot particle shapes were modeled by assuming microphysical constraints on the particle structure and the geometrical features of sampled aerosols. For the mineral dust model, we neglected the size dependence of particle shape irregularities because of the small number of dry dust samples. Because the surface roughness of dust particles is likely important in determining their optical properties, in future work, the size dependence of the shape properties of dust particles should be considered. In addition, the relationship between water-soluble components of particles and their optical effects for dust and soot particles should be investigated. The transmission electron microscopy tomography imaging technique is expected to be useful for three-dimensional shape modeling of internal mixtures of such aerosols.

1   Yang, P. and K. N. Liou, 1996: Geometric-optics-integral-equation method for light scattering by nonspherical ice crystals, *Appl. Opt.* **35**, 6,568-6,584.

2   Masuda, K., H. Ishimoto, Y. Mano, 2012: Efficient method of computing a geometric optics integral for light scattering by nonspherical particles, Papers in *Meteorology and Geophysics.* **63**: 15-19.

3   Ishimoto, H., Y. Zaizen, A. Uchiyama, K. Masuda and Y. Mano, 2010: Shape modeling of mineral dust particles for light-scattering calculations using the spatial Poisson-Voronoi tessellation, *Journal of Quantitative Spectroscopy & Radiative Transfer.* **111**, 2,434-2,443.

4   Ohser, J. and F. Mücklich, 2000: Statistical analysis of microstructures in materials science, Chichester: John Wiley & Sons.

5   Mikhailov, E. and S. S. Vlasenko, 2006: Podgorny I A, Ramanathan V, Corrigan C E. Optical properties of soot-water drop agglomerates: *An experimental study, JGR.* **111**: D07209, doi: 10.1029/2005JD006389.

6   Ishimoto, H., 2008: Radar backscattering computations for fractal-shaped snowflakes, *Journal of the Meteorological Society of Japan.* **86**, 459-469.

7   Ishimoto, H., K. Masuda, Y. Mano, N. Orikasa and A. Uchiyama 2012: Irregularly shaped ice aggregates in optical modeling of convectively generated ice clouds, *Journal of Quantitative Spectroscopy & Radiative Transfer.* **113**, 632-643.

8   Nakajima, T. and M. Tanaka, 1986: Matrix formulations for the transfer of solar radiation in a plane-parallel scattering atmosphere, *Journal of Quantitative Spectroscopy & Radiative Transfer.* **35**, 13-21.

Single particle analysis of aerosols and cloud residues in the Arctic troposphere

Atsushi Matsuki[1,*], Alfons Schwarzenboeck[2], Boris Quennehen[2], Karine Deboudt[3], Guy Febvre[2], Olivier Jourdan[2], Christophe Gourbeyre[2] and Jean-François Gayet[2]

[1]Institute of Nature and Environmental Technology, Kanazawa University, Kakuma, Kanazawa, Ishikawa 920-1192, Japan
[2]LaMP, Université Blaise Pascal, Clermont-Ferrand II, 24 avenue des Landais 63171 Aubière, France
[3]LPCA, Université du Littoral Côte d'Opale, 189A avenue Maurice Schumann, 59140 Dunkerque, France

*Corresponding author. Tel.: +81 76 264 6510, Email address: matsuki@staff.kanazawa-u.ac.jp (A. Matsuki)

The compositions of individual cloud residues and interstitial aerosol particles collected in northern Scandinavia during the POLARCAT 2008 spring campaign were investigated. Individual aerosol particles and residues from various clouds (ice, liquid, or mixed phase) extracted by an aircraft-borne counterflow virtual impactor were analyzed by both scanning and transmission electron microscopy systems equipped with energy dispersive X-ray detectors. Supermicrometer-sized residues of clouds containing ice crystals tended to be dominantly clay-like mineral dust, whereas marine particles were relatively more important within lower altitude, liquid-phase clouds, indicating distinctly different interactions of different particle types with Arctic clouds. Submicrometer-sized biomass burning (BB) particles (enriched in potassium and often internally mixed with soot) were characteristically found in polluted air masses in the Arctic troposphere. BB particles were also extracted from liquid-phase clouds, and less frequently from ice-phase clouds. In contrast, mineral dust, bare soot, fly ash, and K-rich marine particles dominated submicrometer-sized ice-phase cloud residues. These results suggest that BB particles may be efficient cloud condensation nuclei but their internal mixing can delay or inhibit the ice nucleating properties of bare soot particles. These results show that continental particles are actively transported to the Arctic, where they interact with Arctic clouds.

Keywords: Aerosol particles; Cloud residues; Single particle analysis; Aircraft; Cloud condensation nuclei; Ice nuclei

1. Introduction

In the past 100 years, average Arctic temperatures have been rising at almost twice the rate of temperatures in the rest of the world [1], and global circulation models agree that Arctic warming will continue to exceed the global mean warming [2]. High surface albedo in the Arctic region can amplify both the direct and indirect radiative effects of aerosols. Over the ice, even weakly absorbing aerosol layers can heat the Earth/atmosphere system [3], making the Arctic climate especially vulnerable to any changes in aerosol and cloud microphysical properties.

POLARCAT (POLar study using Aircraft, Remote sensing, surface measurements and modeling of Climate, chemistry, Aerosols and Transport) is an international program endorsed as part of the 4th International Polar Year (2007–2008), which aims to quantify the impact of trace gases, particulate aerosols, and heavy metals transported to the Arctic and their contribution to pollutant deposition and climate change in the region. The POLARCAT-France team used in situ aircraft measurements to better quantify the impact of aerosol particle properties on cloud characteristics in the Arctic during the spring 2008 campaign. The focus of this particular study is the detailed characterization of individual cloud residual and interstitial aerosol particles collected with an airborne counterflow virtual impactor (CVI) to provide insights into the cloud nucleating properties of Arctic aerosols.

2. Methods

The ATR-42 research aircraft was stationed at Kiruna airport (67°50′N, 20°20′E, 460 m a.m.s.l.) in northern Sweden from 30 March to 11 April 2008 during the POLARCAT-France spring measurement campaign. The aircraft made multiple level flights when cloud layers and pollution plumes were present in the low to mid troposphere (0.3–6 km). Tropospheric aerosol particles as well as residues from

various clouds (ice-, liquid-, or mixed-phase) extracted by the CVI were analyzed later in the laboratory on an individual particle basis by both scanning and transmission electron microscopy systems equipped with energy dispersive X-ray detectors (SEM- and TEM-EDX systems).

3. Results and discussion

Supermicrometer-sized residues of clouds containing ice crystals tended to be dominantly clay-like mineral dust, whereas marine particles were relatively more important within lower-altitude liquid-phase clouds, indicating distinctly different interactions of the different particle types with Arctic clouds.

Submicrometer-sized biomass burning (BB) particles (enriched in K and S and often internally mixed with soot) were characteristically found in polluted air masses in the Arctic troposphere (Figures 1 and 2). BB particles were primarily extracted from liquid-phase clouds and less frequently from ice-phase clouds. In contrast, mineral dust, bare soot, fly ash, and marine (sea salt, often enriched in K) particles dominated submicrometer-sized ice cloud residues. These results suggest that BB particles may be efficient cloud condensation nuclei (CCN) but that their internal mixing can delay or inhibit the ice nucleating properties of bare soot particles. These results show that continental particles are actively transported to the Arctic, where they interact with the Arctic clouds.

Mineral dust (Al, Si, Fe)   Fly ash (Al, Si, Fe)

Marine (Na, Mg, S, Cl, K, Ca)   Marine (K-rich)

Soot (C only)   Sulfate (S)

Biomass burning particles (S, K) with soot inclusions
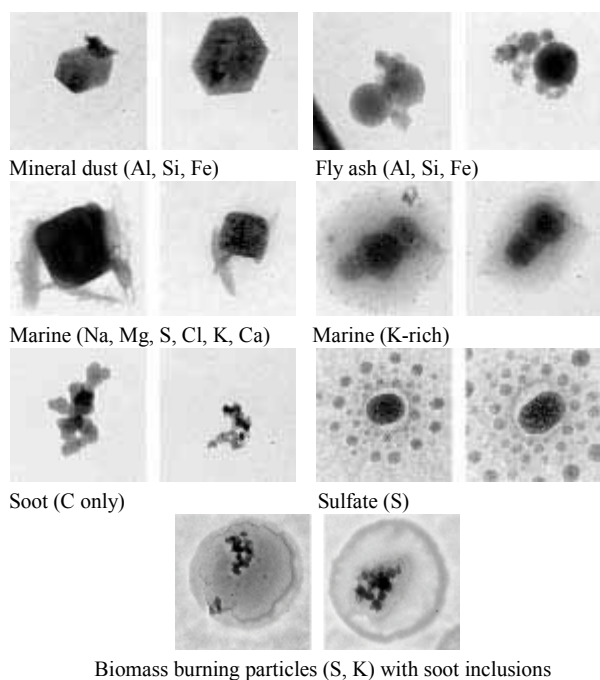
Figure 1 Representative TEM images of submicrometer-sized cloud residual and aerosol particles collected during the POLARCAT-France spring measurement campaign. Particle types were distinguished by their characteristic morphology and the elements detected by EDX. Each image is 500 nm wide.
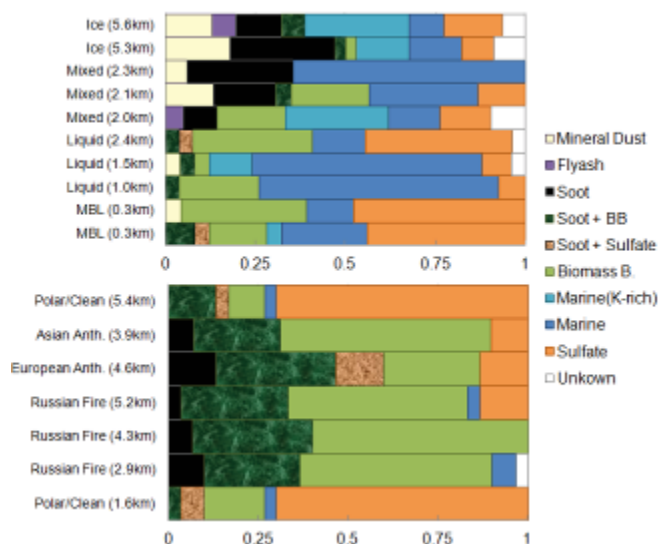
Figure 2 Relative abundance of particle types among submicrometer-sized cloud residues (ice, mixed, and liquid phases) and aerosols in the marine boundary layer (upper panel), following manual identification by TEM-EDX analysis. The particle types of free tropospheric aerosol particles collected under polluted and clean Arctic conditions [4] are also shown for comparison (lower panel).

The enrichment of marine particles in ice- and mixed-phase residues and the abundance of BB particles in interstitial aerosols found in this study are surprisingly consistent with the results of CRYSTAL-FACE experiments [5], which found a high abundance of sea salt in ice residues but a low quantity in interstitial aerosols. Conversely, the vast majority of interstitial aerosol particles, but not ice residues, were BB-related particles (those with mass spectral features of sulfates, K^+, organics, and NO^+). This similarity is striking considering the different analytical methods used and the different geographical settings (i.e., cirrus clouds at 13 km over Florida).

1 Intergovernmental Panel on Climate Change, Climate Change 2007: The Physical Science Basis, in: Contribution of Working Group I to the Fourth Assessment Report of the Intergovernmental Panel on Climate Change, *Cambridge Univ. Press.* Cambridge, UK, 2007.

2 ACIA, 2004: Impacts of a Warming Arctic, Arctic Climate Impact Assessment, *Cambridge Univ. Press*.

3 Pueschel, R. F. and S. A. Kinne, 1995: Physical and radiative properties of Arctic atmospheric aerosols, *Sci. Total Environ.* **160/161**, 811-824.

4 Quennehen, B., A. Schwarzenboeck, A. Matsuki, J. F. Burkhart, A. Stohl, G. Ancellet and K. S. Law, 2012: Anthropogenic and forest fire pollution aerosol transported to the Arctic: observations from the POLARCAT-France spring campaign, *Atmos. Chem. Phys. Discuss.* **12**, 4,541-4,588.

5 Cziczo, D. J., D. M. Murphy, P. K. Hudson and D. S. Thomson, 2004: Single particle measurements of the chemical composition of cirrus ice residue during CRYSTAL-FACE., *J. Geophys. Res.*, **109**, D04201.